STYRELSEN FÖR

VINTERSJÖFARTSFORSKNING

WINTER NAVIGATION RESEARCH BOARD

Research Report No 40

THE ATMOSPHERIC BOUNDARY LAYER OVER THE BOTNIAN BAY: A REVIEW OF WORK ON MOMENTUM TRANSFER AND WIND STRUCTURE

BY SYLVAIN M. JOFFRE

Sjöfartsstyrelsen
Finland

Finnish Board of Navigation

Sjöfartsverket
Sverige

Swedish Administration
of Shipping and Navigation

THE ATMOSPHERIC BOUNDARY LAYER OVER THE BOTHNIAN BAY: A REVIEW OF WORK ON MOMENTUM TRANSFER AND WIND STRUCTURE

Sylvain M. Joffre(*)

Institute of Marine Research
PB 33, 00931 Helsinki, Finland

(*) Current affiliation: Finnish Meteorological Institute
Aerological department,
P.B. 50, 00811 Helsinki, Finland.

ISBN 951-46-8314-5

Helsinki 1984. Government Printing Centre

F O R E W O R D

A problem encountered while developing forecasting methods for sea ice behaviour is the interaction between the atmosphere and the ice.

The Winter Navigation research Board herewith presents its report no 40, which is devoted to this problem.

We thank the author and his colleaques for a fine job.

Helsinki and Stockholm, August 1984

Jan-Erik Jansson Kaj Janérus

A B S T R A C T

Investigations carried out with a view to promoting our understanding and the parameterization of momentum transfer between the atmospheric boundary layer and the ice-covered Bothnian Bay are reviewed. The scientific results from three field experiments are summarized and conclusions are drawn concerning the dependence of the cross-isobar angle and drag coefficients or wind ratios on thermal stratification, baroclinity and inertial effects. Implications for wind modelling are discussed, and an example of the application of this approach with a simple statistical model using a new wind predictor is given. This approach is supported by a short sequence of observational data. Wind statistics from the field experiments, an automatic weather station and local wind analyses are compared. In conclusion, possible routine schemes for wind predictions are discussed and recommendations for future work are given.

1. INTRODUCTION

Anyone who makes his living from the sea or who spends much time by or on the sea knows the unpredictability of marine weather and the strong interaction between the atmospheric and the oceanic motion and in return the oceanic heat reservoir is a never-ending source of energy for atmospheric disturbances. Wind forcing at the sea surface generates surface waves, drift currents and ice, or any other, drift (e.g., oil, boat, etc.); in addition the wind can influence the oceanic interior flow via nonlinear processes. Maritime activities depend to a great extent on the state of the sea, and thus, prediction of the wind field above the sea and our ability to grasp the exchange of momentum, heat and mass

between the two media is more than a purely academic exercise; it is a problem of economics, too.

Technological advances with more powerful machinery, new navigation systems and increased automatization on board ship have permitted year-round, all-weather maritime activities to be extended to ever more remote locations (e.g. the Arctic Ocean) in response to the requirements of a developing economy. However, safety and efficiency still require forecasting the behaviour of atmospheric and oceanic flows.

Unfortunately, observations at sea are rare and most of them are from coastal stations, which we now know are biased by local factors (e.g. Joffre & Makkonen, 1981; Weisberg & Pietrafesa, 1983). This puts extra emphasis on the theoretical approach, which is the only way that the basic physical processes can be described and explained. Only afterwards can observational and statistical elements be added to provide numerical estimates for our problem.

Since 1975, the Finnish Board of Navigation has been giving financial support to a research project carried out at the Institute of Marine Research (IMR), Helsinki, with the primary aim of clarifying the nature and magnitude of the basic processes involved in the interaction between the atmosphere and the sea ice fields in the Bothnian Bay. A large proportion (17 %) of Finnish exports pass through the harbours of the Bothnian Bay, the most northern part of the Baltic Sea, which freezes completely for approximately five months every winter.

The secondary aim of these theoretical investigations was to enable us to predict more accurately the wind field on the mesoscale(†). At the same time, research was initiated to develop an ice-drift model that could be used for icebreaker activities in the northern part of the Baltic Sea (Leppäranta, 1981). The grid-mesh of this model was 27 km, i.e. on a meso-β scale (L ∿ 20-200 km).

(†) Mesoscale (L ∿ 2-2000 km) refers here to subsynoptic scales. Weather forecasts are usually made on a synoptic scale, i.e. L > 2000 km (Orlanski, 1975).

The two sets of research cooperated in investigating the possibility of providing wind data for the ice model on the smallest scale possible and in providing insight into the parameterization of the wind forcing term in the model.

This research project has now reached the final stage for the theoretical and empirical aspects of momentum transfer parameterization between wind and ice. Numerical values for transfer coefficients can be presented here with their physical dependences as well as more physical understanding for the failure of certain parametrization schemes. The wind field distribution problem has been investigated from the point of view of the search for specific wind concepts freed from disturbing factors, since the nature of our data was such that they did not permit more general statistical investigation. The data bases required for continuation and extension of this investigation to a suitable wind format for ice model assimilation, including horizontal spatial variability, are held by the Finnish Meteorological Institute (FMI); closer cooperation with this Institute is therefore recommended.

The purpose of this report is to relate the work done and the results achieved at this turning point in the investigation. We shall first describe the theoretical background and identify the problems and then present the methods available to solve them (section 2). Then, the experimental work carried out in order to document the various processes will be described with some comments on their success and drawbacks (§ 3). Section 4 will present the main results of these empirical investigations in their theoretical framework. The next step is to document statistically (or climatologically) our knowledge of wind conditions in order to extract certain general patterns of behaviour and easy-to-reproduce features (§ 5). In section 6 we shall present some results of wind modelling with emphasis on the relative importance of predictors. Finally, section 7 will summarize the achievements and the shortcomings of the work in order to provide recommendations for using the results of this research and for future work pertinent to this problem.

2. STATEMENT OF THE PROBLEM

2.1 Background

Any flow sweeping over a surface must adjust to the surface conditions (roughness, surface temperature and surface wetness). The difference in the properties of the two media (here the atmosphere and the sea surface) and the viscidity of the medium makes this adjustment layer have a non-infinitesimal thickness and be the location of very important physical processes. This adjustment layer, called the atmospheric boundary layer (ABL), acts as a buffer layer between the free atmosphere above and the surface beneath. All the characteristics of this layer (and unfortunately all its difficulties) arise from the fact that it is always in a state of turbulent motion.

Above the ABL is the free-stream (frictionless) large-scale flow in which the basic balance is between the pressure-gradient and the Coriolis forces, this equilibrium being destroyed transiently by advection of momentum and vorticity embedded in the atmospheric disturbances. This large-scale flow velocity V_{LS} acts as an external driving force for the ABL flow. The wind and temperature profiles within the ABL tend towards the free-stream values that they reach at the top of the ABL denoted by h. Below, the velocity tends towards zero (or towards the drift current velocity) at the surface while the temperature adjusts itself to the surface temperature as does the humidity (see Fig. 1).

Now, either the potential temperature increases with height (profile $\Theta^{(1)}$) and the stratification is stable or the potential temperature decreases with height ($\Theta^{(2)}$) and the situation is hydrostatically unstable. In the former case, turbulent fluctuations are weak and the wind shear is large in a relatively thin ABL (typically 50-500 m), in the latter case strong convective fluctuations mix the ABL efficiently, resulting in a thicker well-mixed layer (typically 200-2000 m). However, the unstable case observations described in this report did not correspond to a pure convective state but rather to a dual production state with both mechanical and thermal mixing. Thus, the sign and the magnitude

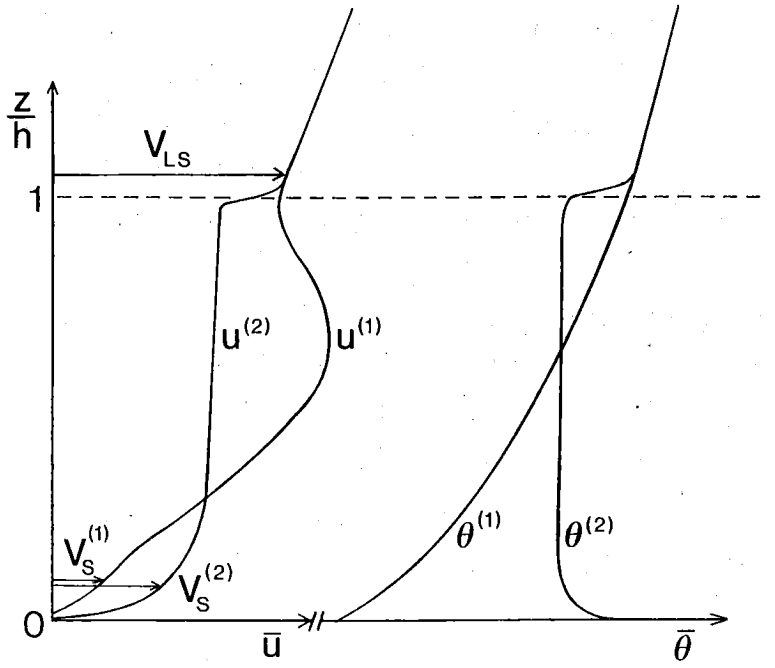

Fig. 1: Schematic representation of wind ($\bar{u}$) and potential temperature ($\bar{\Theta}$) vertical profiles under stable (1) and unstable (2) conditions. The vertical coordinate z is non-dimensionalized with the ABL height h.

of the potential temperature gradient are the primordial ingredient shaping wind profiles and tagging the physical structure of the ABL. From a practical point of view, note that in the stable case the surface wind velocity is much smaller than the basic flow velocity above whereas in the unstable case these two velocities are much closer.

2.2 Theory of the methodology

Now the basic problem is to get the wind close to the surface, say, at a reference level z = 10 m (the surface wind V_s), knowing only the large-scale flow or an approximation of it called the geostrophic wind V_g. This geostrophic wind is a theoretical concept rather than an observable wind: it assumes a perfect balance

between the pressure-gradient and the Coriolis force (connected to the rotation of the earth) without frictional influences. Moreover, it is generally determined at grid points 150 km apart, which is roughly the width of the Bothnian Bay. Thus, the analysis techniques involved in determining V_g will smooth out any irregularities, and many of the details, e.g. curvature in the streamlines, are lost. On the other hand, these techniques can add artificial features to the field analysed, thus causing errors that may even grow with time. If these subgrid ($\lesssim$ 150 km) details increase for some hydrodynamical reason and enhance existing disturbances they may be very important, resulting in unpredictable (and unpredicted) damage such as that caused by the recent "Mauri-myrsky" event in Northern Finland.

Thus, we must interpolate the upper wind downwards to obtain V_s. The vertical profile of the longitudinal component $\bar{u}(z)$ of the wind, i.e. the rate of decrease in the wind velocity downwards, will be determined primarily by the roughness of the surface and the hydrostatic stability of the layer. Further, the state of the large-scale flow will also influence the profiles (through baroclinity and inertial effects). On the other hand, the earth's rotation causes the wind to turn with height, so that there is also a lateral component $\bar{v}(z)$ which must be estimated or predicted. The total turning between the surface wind direction α_s and the geostrophic wind direction α_g (i.e. along the isobars) is called the cross-isobaric angle α_o and is defined positive towards lower pressure although the veering is clockwise in the Northern Hemisphere. The turning α_o will depend on surface roughness and stability and to the second order on baroclinity and acceleration. Throughout this study we take the x-axis along the surface wind.

However, knowledge of the surface wind is not the end of the road. Although V_s is needed for ship navigation, pleasure sailing, icebreaker activity, etc., oceanography and other practical applications such as wave development, current and ice- and oil-drift predictions require knowledge of the rate of downward momentum transfer from the atmosphere to the sea. This is determined by

the shape of the profile between V_s and the surface. This momentum input is also called the surface stress τ_o. In fact, it is more practical to use the concept of friction velocity u_* to express this stress since

$$\tau_o = \rho_o \, u_*^2 \qquad (1)$$

where ρ_o is the air density which is almost constant ($\cong 1.2$ kg/m^3). The determination of u_* requires either direct measurements of turbulent fluctuations at 1-10 Hz (with sophisticated sensors providing a large body of data and necessitating time-consuming digital processing) or measurements at several levels (at least four or five below 10 m) close to the surface in order to know accurately the shape and slope of the wind profile. Since such measurements are not available on a routine basis, the only way is to parameterize the stress. From laboratory experiments, we use the relation

$$u_*^2 = C_D \, V_s^2 \qquad (2)$$

where C_D is a dimensionless bulk parameter, the drag coefficient. Thus, if the surface wind is known (observed or predicted), knowledge of C_D is enough for determining the stress. Unfortunately, the drag coefficient is strongly dependent on thermal stability, on roughness, on the height of observations and also on non-local effects advected by the wind. A large body of observations has been gathered concerning the variability of C_D. Although the mean trends of its behaviour are known, there is still a large scatter in the observations, shading somewhat its representativeness.

To avoid the additional step of the surface wind, the stress can be obtained directly from the large-scale flow in the equivalent format

$$u_*^2 = C_g \, V_g^2 \qquad (3)$$

or

$$u_*^2 = C_{LS} \, V_{LS}^2 \qquad (4)$$

where C_g and C_{LS} are the corresponding geostrophic and upper flow drag coefficients, respectively. The parameters C_g and C_{LS} depend on stability and roughness but definitely also on baroclinity and acceleration, although the latter two are generally discarded in most studies. The scatter in C_g values is also large mainly because of uncertainties in the determination of V_g and the non-incorporation of disturbing effects such as baroclinity and inertial effects. Although these latter influence surface values (V_s and C_D) as well they are less essential there since turbulence time-scales are much shorter close to the surface and a continuous quasi-adjustment takes place. At higher levels, turbulence scales become comparable to the characteristic time-scale of the changes of the flow, and their effects can no longer be neglected. Note that the link between input data and the stress is shorter for the upper wind method and in a way smoothes out the variability present in the profiles. On the other hand, the range of variability in C_D and V_s is smaller and thus large errors, implying complete predictive failure, are less probable.

An important issue is the question of non-homogeneity in surface conditions when, for instance, the ice field of different sized-floes is also cut by open leads. The direct contact of cold air with water results in strongly enhanced heat exchanges (Topham et al., 1983, p. 2889), up to 20-30 % of the total exchange in spite of their relatively small areas. Thus, it would be important to know the relative location of meteorological instruments with respect to these transitional features, since downwind observations would register convective structure and low roughness conditions advected in a developing internal boundary layer (Andreas et al., 1979).

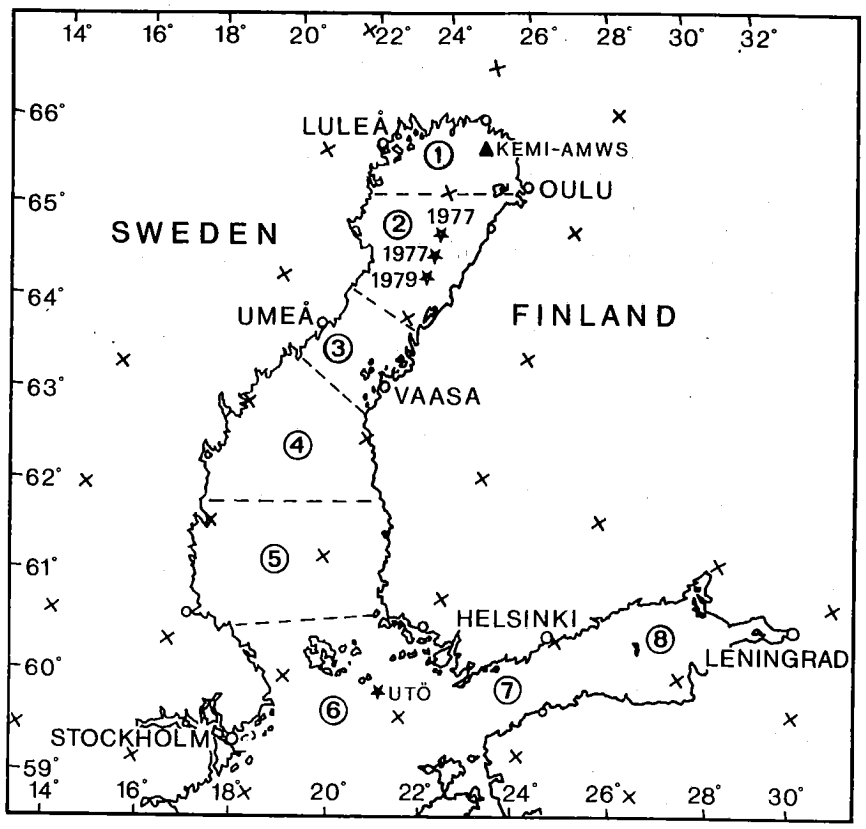

Fig. 2: Location of the field experiment sites described in this report (stars). The encircled numbers designate the sea areas for local wind forecasts from the FMI. The crosses indicate the grid points at which the surface pressure field is analysed.

3. DATA AND EXPERIMENTS

3.1 The Utö data

A total of 250 pilot balloon profiles performed in 1930-36 on the island of Utö (see Fig. 2) were analysed in order to determine the large-scale stress over the sea in the vicinity of Utö for both ice-free and ice-covered situations (Joffre, 1978). Although the presence of the island may distort profiles, the low elevation of the relief and the lack of trees ensure rather good representativity of the sea area.

The lack of good surface measurements was the main limitation in this data set. Both wind V_s and temperature T_a were measured at only one level ($z_V = 15$ m and $z_T = 2$ m, respectively); the water near-surface temperature T_w was observed during open water periods. The main shaping factor for wind profiles, the hydrostatic stability, was estimated through a bulk Richardson number

$$Ri = \frac{g}{T_a} \frac{T_a - T_w}{V_s^2} \frac{z_V^2}{z_T} \qquad (5)$$

The wind data were available at 100-m intervals up to 500 m and upward at 500-m intervals. These data were used for a climatological study of the ABL structure over the sea, especially with regards to vertical thermal conditions (Ri) and horizontal large-scale thermal influences (baroclinity) whose trace can be analysed from the slope of the wind profiles above the ABL. This study gave the dependence of C_D, C_g and α_o on thermal stability and the orientation β_o of the baroclinity (see § 4.2.4). However, the main result from this analysis was the substantiation provided for the analytical method developed for extracting important information on the structure of the ABL from simple data. Note that the analysed profiles cover only some selected winter situations and a large amount of profiles is still left for potential investigators.

3.2 The 1977 ice field experiment (ISABLEX-77)

In March-April 1977 a joint Finnish-Swedish expedition performed meteorological, oceanographic and ice structure observations off Raahe-Kalajoki in the Bothnian Bay ($\sim 64^{\circ}30'$ N, $\sim 23^{\circ}$ E). R/V Aranda was moored in the ice field and drifted along with it. The first period of this Ice-Sea-Atmosphere Experiment (ISABLEX) lasted six days and the second phase nine days; the party had to move to another floe in between when the first one disintegrated in a storm. The meteorological data base consists of: mean wind and temperature measurements at five levels between 1 and 10 m from

a mast standing in the middle of a smooth large ice floe (about 2 km in diameter); wind fluctuations at 10 m from a Gill anemometer recorded on photographic paper tape; ice temperature at four levels; wind, temperature and humidity profiles up to 3 km from low-level Vaisala radiosondes (28 profiles) and finally about 100 pibals giving wind profiles up to at least 500 m. A 13-m^3 kytoon was also launched giving 10 profiles up to 400-500 m under weak wind conditions. The turbulent data from the Gill anemometer have not been analysed owing to the lack of personnel for the cumbersome task of digitizing the recording tape.

The mast profiles enable us to study the fine structure of the profiles close to the surface and the rate of downward momentum transfer as a function of stability conditions. The variations in the smooth roughness conditions were also studied under various flow conditions. The upper profiles gave a good representation of the structure, height and evolution with time of the whole ABL as a function of turbulence conditions. These profiles were also used to parameterize the height of the ABL. The large-scale roughness was determined, as with the Utö data, but now we had the advantage that it could be compared with the skin roughness determined from the mast data. The difference between them was attributed to the effect of large-scale roughness elements (ice ridges and hummocks), whose rough statistical distribution was estimated separately.

These data have also been used to estimate the influence of large-scale disturbances (baroclinity and acceleration) on the averaged characteristics of the ABL. Moreover, using the pressure field analysis of the FMI we were able to correlate the ABL flow and the surface wind to the external geostrophic flow. Using these statistics we could develop a prediction model of the surface wind.

3.3 The 1979 ice field experiment (ISABLEX-79)

In April 1979 a second rather similar expedition was undertaken near Ulkokalla ($\sim 64^{\circ}$ 20' N, $\sim 23^{\circ}$ 05' E) in the Bothnian Bay. This time a 16-m mast was used with six levels of instrumentation down

to 0.6 m. The data were more valuable than those gathered in 1977 since temperature and wind direction were registered at a 1-min^{-1} frequency instead of 0.1-min^{-1} as in 1977. Wind direction and global radiation were each observed at two different levels along the mast. Ice and snow temperature were recorded at five different levels. Upper profiles were similarly performed with both radio and pilot soundings. These data have not been analysed from the point of view of the turbulent structure but only to implement the statistical study started in 1977 on wind conditions over the sea. Further information was provided by the geostrophic wind computed from the pressure analysis of the FMI and by the wind observations at the AMWS (Automatic Marine Weather Station) of Kemi. The wind data base created was used to compare the various wind estimates, looking especially for any systematic bias, and to assess whether mutual departures can be related to a certain type of flow or ABL structure.

4. RESULTS

4.1 The wind profile close to the ice surface

4.1.1 Theory

From both laboratory and atmospheric measurements it is known that wind $\bar{u}$, potential temperature $\bar{\Theta}$ and humidity $\bar{q}$ follow a logarithmic profile in the surface, or Prandtl, layer within which Coriolis and pressure-gradient effects are unimportant:

$$\bar{u}(z) = \frac{u_*}{k} \{\ln(z/z_o) - \Psi_u(\zeta)\} \tag{6}$$

$$\bar{\Theta}(z) - \Theta_o = \frac{\Theta_*}{k} \{\ln(z/z_H) - \Psi_\theta(\zeta)\} \tag{7}$$

$$\bar{q}(z) - q_o = \frac{q_*}{k} \{\ln(z/z_E) - \Psi_q(\zeta)\} \tag{8}$$

where an overbar means a suitably defined time-average, z is the vertical elevation, k is the Karman constant (= 0.4), z_o is the

surface roughness length, z_H and z_E are the temperature and humidity roughnesses, $\theta_* = -Q_o/u_*$ is a temperature scale with Q_o the kinematic surface turbulent heat flux, $q_* = -E_o/u_*$ is a humidity scale with E_o the surface evaporation and θ_o , q_o are the surface values of the temperature and humidity. The departure from the pure logarithmic profile because of diabatic effects is expressed by the universal functions Ψ_u , Ψ_θ and Ψ_q depending on the sole dimensionless stability parameter $\zeta = z/L_*$ where $L_* = u_*^2\ \theta_o/g\ k\ \theta_*$ is the Monin-Obukhov length roughly describing the height above which buoyant effects are non-negligible (g is the acceleration due to gravity). These functions tend towards zero when $\zeta \to 0$ ($L_* \to \infty$) and the conditions are adiabatic.

It is widely accepted nowadays that when $\zeta > 0$ (stable stratification)

$$\Psi_u = -\beta_u\ \zeta \qquad \Psi_\theta = \Psi_q = -\beta_\theta\ \zeta \tag{9}$$

and for unstable conditions ($\zeta < 0$)

$$\Psi_u = 2\ \ln\frac{1+X}{2} + \ln\frac{1+X^2}{2} + \frac{\pi}{2} - 2\ \arctan X \tag{10a}$$

$$\Psi_\theta = \Psi_q = 2\ \ln\frac{1+Y}{2} \tag{10b}$$

where $X = (1-\gamma_u\ \zeta)^{1/4}$ and $Y = (1-\gamma_\theta\ \zeta)^{\frac{1}{2}}$. The coefficients β_u , β_θ , γ_u and γ_θ are "universal" constants and should be determined empirically. Present consensus gives $\beta_u \cong \beta_\theta \cong 4\text{-}7$, $\gamma_u \cong 15\text{-}22$ and $\gamma_\theta \cong 9\text{-}18$. This still shows some scatter. Equations (6) and (7) show that fitting a regression line to wind $\overline{u}_i$ and temperature $\overline{\theta}_i$ observations at several levels z_i (i=1,2,3,..) enables us to compute the slopes u_* or θ_* and the intercepts z_o or θ_o. Since the functions Ψ_u and Ψ_θ include, through L_* , the unknowns u_* and θ_* , an iteration technique is necessary (see Table 1).

1. Compute $Ri = (g/\Theta_o)(\partial\overline{\Theta}/\partial z)(\partial\overline{u}/\partial z)^{-2}$
2. Take $\zeta = Ri$
3. Compute Ψ_u and Ψ_θ
4. Fit $\overline{u}_i$ vs. $\ln z_i - \Psi_u(z_i)$
   and $\overline{\Theta}_i$ vs. $\ln z_i - \Psi_\theta(z_i)$
5. Compute $L_*(u_*, \Theta_*)$
6. u_* and Θ_* values converge
   if yes: go to 7
   if no : go to 3
7. End

Table 1: Iteration flow chart for computing the surface turbulent fluxes.

4.1.2 Study of the roughness conditions

For the roughness length z_o describing the smooth ice surface around the mast during ISABLEX-77 we found

$$z_o \cong 0.04\text{-}0.08 \text{ cm} \qquad (11)$$

This range of values is representative of an underlying surface of this type and it agrees with other values obtained elsewhere over ice or snow (see Table 1 in Joffre, 1981, for a compilation of data). Although this parameter z_o partly describes the mean height of surface roughness elements, it is also a boundary condition depending on flow conditions. This second dependence has seldom been investigated. Our results seem to indicate that z_o is stability dependent through a dependence on the Reynolds number. A low Reynolds number under stable conditions gives higher values of z_o (see Joffre, 1982b). The theoretical importance of such a finding is, however, tempered by the fact that the wind is low under strongly stable conditions and the turbulent transfers at the surface are thus weak.

More interesting is the parameterization formula relating roughness to the transfer rate u_* through a square law:

$$z_o = m\, u_*^2 \qquad (12)$$

with $m = 1.5 \times 10^{-5}$ s/cm^2 in agreement with Chamberlain (1983), who found $m = 1.6 \times 10^{-5}$ s/cm^2.

4.1.3 The drag coefficient C_D

The simplest way of parameterizing the stress u_*^2 is through a drag coefficient C_D (see Eq. 2). The dependence of C_D (for a reference level of 10 m) on the stability parameter z/L_* is shown in Fig. 3 from Joffre (1982b). Note the strong variability in C_D with thermal stratification, however, the neutral value is close to 1.5×10^{-3} a typical value found elsewhere. The continuous lines in this figure represent the theoretical dependence of $C_D = (u_*/u_{10})^2$ on ζ given by Eq. (6).

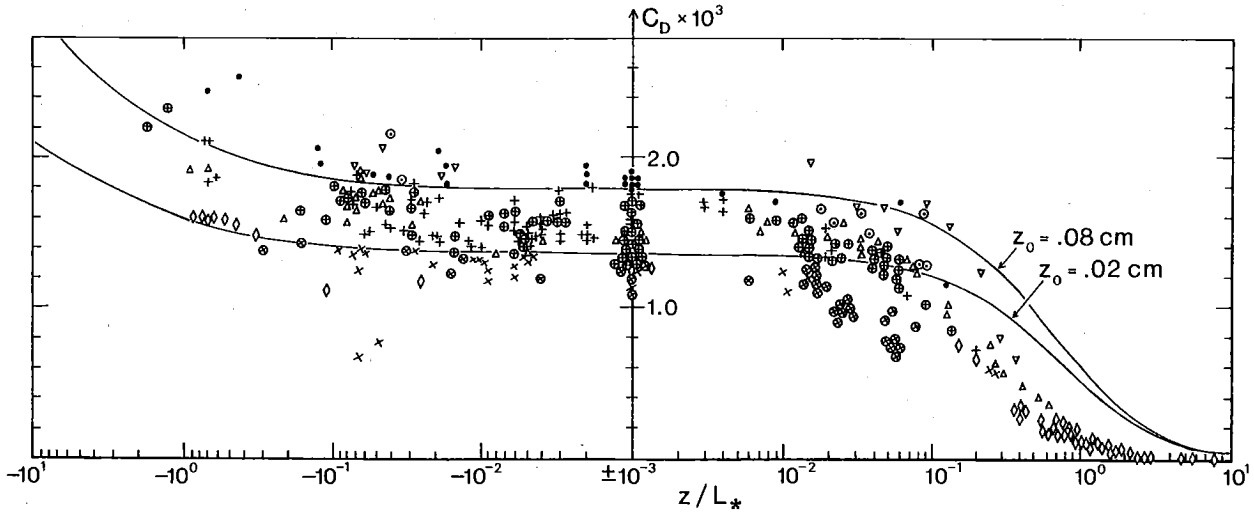

Figure 3: Dependence of the drag coefficient $C_D = (u_*/V_s)^2$ on thermal stability z/L_*. The two continuous lines describe Eq. (6) for two values of the roughness parameter z_o. The different symbols refer to different stationarity conditions (for details see Joffre, 1981).

As a consequence, any model taking C_D as a constant to compute the wind stress at the surface (e.g., Leppäranta, 1981) may result in serious problems in principle. On the other hand, this dependence does not facilitate our task for modelling purposes since we now need knowledge of the thermal structure of the lowest layer of the atmosphere in addition to the wind. In other words, we need temperature data at two levels (see Eq. 5), which is far from being easy, especially in the case of ice-covered sea. We shall come back to this question (see § 7.1).

It has to be noticed that stability defined from routine observations with a Richardson number Ri (Eq.(5)) can be readily trans-

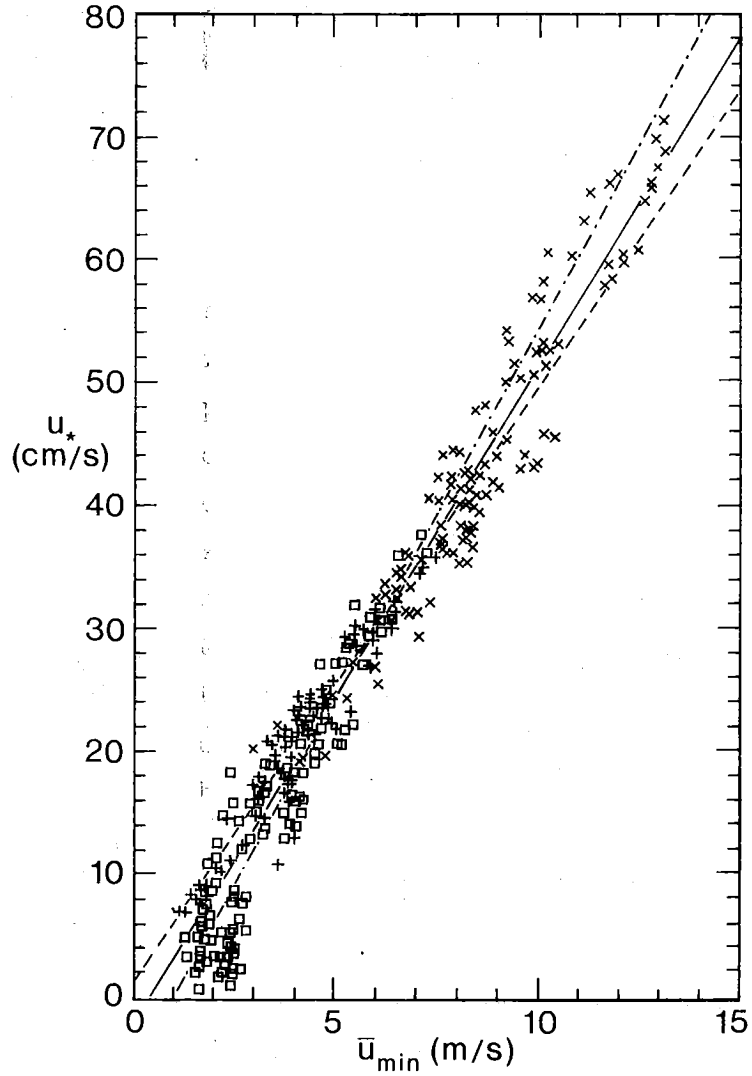

Figure 4:

Empirical dependence of the friction velocity u_* on the 1-m level wind $\bar{u}_{min}$. (□ -.-·-□) stable conditions, (×——— ×) near-neutral conditions and (+- - -+) unstable conditions.

formed into the universal stability parameter ζ which enters the general flux-profile expressions (Eqs. (6)-(10)).

This annoying stability dependence can be avoided if one takes the reference level z_{ref} at a lower height, where buoyant effects do not intervene, i.e. $z_{ref} \ll L_*$. Taking z_{ref} at our lowest observation level of 1 m, we found a nice linear trend (see Fig. 4) independent of stability. We shall make good use of this method in § 6.2. Note that the corresponding picture with u_* vs. $\bar{u}_{10}$ shows a large scatter.

4.1.4 The large-scale roughness

The stress determined from the mast measurements is representative of only a small area upwind of the mast. However, the wind field in the bulk of the ABL "feels" the integrated effect of all roughness elements, small and large. Consequently, in order to observe the signature in the wind profile of this integrated effect, we have to consider the upper part of the profiles as well. We use the geostrophic departure method, i.e. the cross-isobaric flow is vertically integrated from the surface, where the stress is now an overall value U_*^2, to the top of the ABL, where the stress vanishes. The main flaw in this method is that the upper profiles consist of instantaneous observations, and these cannot be a good sample of the random movements of the rising balloon following individual eddies. Moreover, the computation procedure assumes that the situation is stationary and that there are no entrainment processes. The stationarity constraint is relaxed by dealing with mean profiles; the rate of entrainment was generally small in our non-convective observations.

We can write

$$U_*^2 = u_{*s}^2 + F_D \qquad (13)$$

where u_{*s}^2 is the local stress determined from mast measurements (see § 4.1.1) and F_D is the unknown form drag due to pressure differences on both sides of large roughness elements such as

	Site 1	Site 2
F_D/U_*^2	0.59	0.27
μ (km^{-1})	7.6	3.0
$\lambda \times 10^3$	3.57	0.87

Table 2: Empirical average values of the relative share of form drag to total drag (F_D/U_*^2), of the mean frequency μ and of the roughness concentration parameter λ for the two sites of ISABLEX-77.

ridges and hummocks. It is important to relate this form drag contribution to the statistical distribution of these roughness elements. It was shown in Joffre (1983a) that F_D was well correlated with the mean frequency μ (in km^{-1}) of ridges observed from helicopter flights (see Table 2).

Furthermore, it was shown that the share of F_D in U_*^2 increases with increasing stability, probably because of the incapacity of the turbulent field to compensate for increased momentum loss. On the other hand, surface layer models predicting F_D from ice statistics seem to underestimate its share, thus stressing the importance of dealing with the whole profile. Since these profiles fluctuate considerably and are uncertain, it would be very valuable to perform aircraft crossings at several levels and to measure the intensity of turbulence at these levels together with ice statistics surveys.

Arya (1973) has shown that the dimensionless parameter $\lambda = \mu h_s$ (with h_s the average roughness element height) is very important in the parameterization of the form drag. Figure 5 illustrates the dependence of the normalized dimensionless ratio $(F_D/U_*^2)/\lambda$ on thermal stability. Here the stability parameter h/L_* involving the ABL height h is more relevant than the parameter z/L_* since h is also coupled with the overall roughness, and the bulk effect of the roughness element extends up to heights comparable to h. It has to be pointed out, however, that this stability dependence

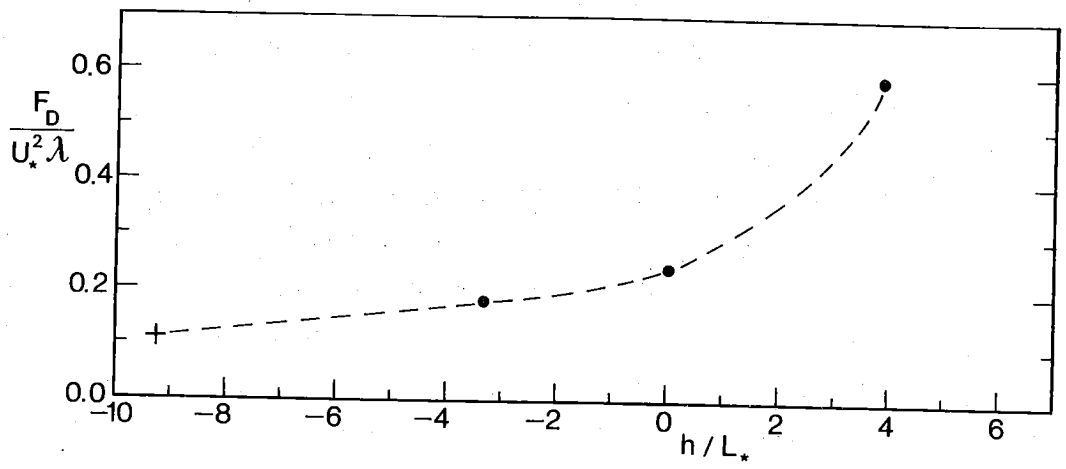

Fig. 5: Dependence of the scaled dimensionless form drag contribution to the total stress U_*^2 on thermal stability h/L_*. (+) site 1 and (•) site 2 of Isablex-77.

is a consequence of the fact that the local stress decreases with departure from adiabatic conditions rather than that the total stress U_*^2 varies with stability. Including F_D, we found that the neutral overall roughness Z_o is approximately one order of magnitude larger than z_o, i.e. 0.15-0.4 cm, and C_D would be 20-50 % larger, i.e. $1.8\text{-}2.3 \times 10^{-3}$.

4.2 The bulk of the ABL

4.2.1 Theory

Although the theoretical basis for expressing the wind, temperature or moisture profiles in the surface layer is rather sound and supported by empirical data, the situation is not so satisfactory above the surface layer (approximately 10 % of the whole ABL) within the bulk of the ABL. In the surface layer, the internal time scale of the turbulence field was rather short, allowing rapid adjustment to various external forcings. However, this scale grows with elevation and thus becomes comparable with new relevant scales such as those connected with the rotation of the

earth, thermal wind (i.e. baroclinity) and acceleration or advective effects. This means that one cannot derive general analytical expressions for the profiles. Moreover, observations in the upper layers of the ABL are less accurate since they are generally obtained from balloon tracking. The similarity theories define only the dimensional relationships to be expected for the variations in the profiles. Thus, it is more beneficial to try to connect the wind field close to the surface (or the surface stress) to the wind field capping the ABL, i.e. towards which the profile tends asymptotically. This can also be done theoretically using the resistance laws. However, they include universal functions (functions A and B, see Arya, 1977), which are rather poorly known and although we have determined them from our data, the scatter encountered inclined us not to consider them in this report (see Joffre, 1981, 1982a and 1984b).

When speaking about the wind (or temperature) at or above the top of the ABL, we imply that we know this height h which will be used as a reference level for the upper wind. This brings us to a second problem: how can this ABL height h depending on time, weather conditions and internal structure of the ABL be either observed, diagnosed or predicted.

4.2.2 The upper wind

Above the ABL where friction effects are negligible, we have geostrophic equilibrium under conditions of stationarity and horizontal homogeneity. Because of this balance between the Coriolis and pressure-gradient forces we can define the geostrophic wind V_g from the pressure field. We computed V_g by fitting a second-order surface regression to the analysed surface pressure field of the FMI on a 15×9 grid over northern Europe (with a mesh of 150 km) and then interpolated it to the location of R/V Aranda. If the situation is barotropic, i.e. the pressure and density surfaces coincide, the pressure gradient is conserved with height.

Unfortunately, such a simple state does not always occur and advective terms in particular can be important. The observed upper wind V_{LS} includes implicitly such disturbing effects and might be a better predictor for surface flow conditions. However, it is not a very accurately quantity but, on the other hand, it is becoming available from numerical models.

A third wind concept needs to be presented here; this is the vertically integrated wind <V> such that

$$\langle V \rangle = \frac{1}{h} \int_0^h V(z)\, dz \qquad (14)$$

which is a bulk wind expressing the mass flow through the ABL. Note that numerical model outputs also correspond to integrated values between grid points. On the basis that the mass flow in the ABL is grossly conserved whatever the flow conditions, we can expect <V> not to be affected by baroclinity or a different state of hydrostatical stability even though the shape of the profiles may be much altered. The vertical integration acts somewhat as a filter.

Obviously, the main problem with <V> is its determination since complete profiles V(z) are not generally available. We therefore need statistical relationships between <V> and V_g or $V_{LS}(h)$ (see Fig. 6). We need more data of this sort before reliable empirical relationships can be derived. The relationship between <V> and V(h) can also be derived semi-empirically using the exponent p of the power-law profile (Joffre, 1984a)

$$\langle V \rangle = \frac{V(h)}{p + 1} \qquad (15)$$

Since the exponent p is not a universal parameter it depends on the flow Reynolds number $Re = z\,V/\nu$ and on the surface Rossby number $Ro = V/f\,Z_o$ in addition to its normal dependence on h/L_* and $h\,f/U_*$ (ν is the molecular viscosity and f the coriolis parameter).

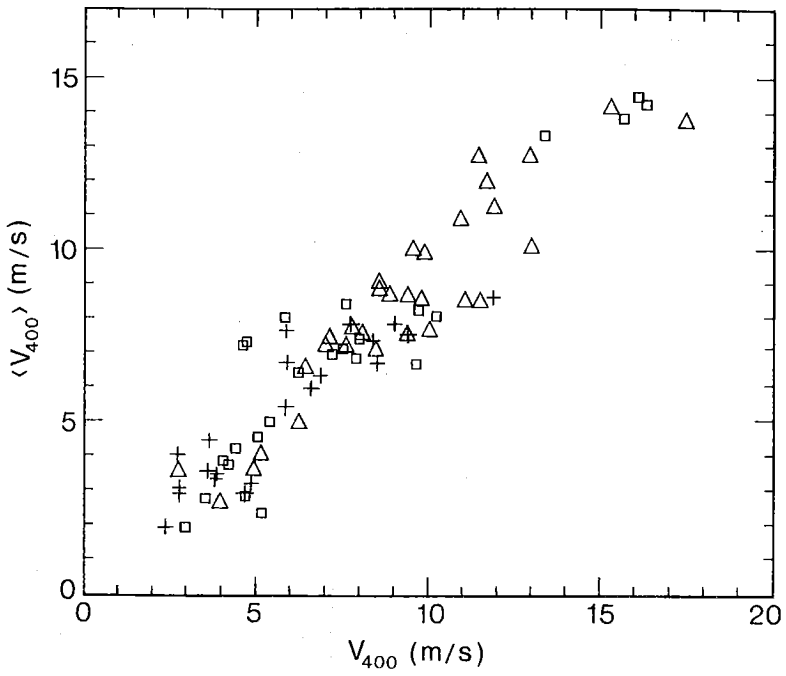

Fig. 6: Scatter diagram between the observed wind V_{400} at z=400 m and the vertically averaged wind $\langle V_{400} \rangle$ between the surface and the 400-m level. (□) stable, (Δ) near-neutral and (+) unstable conditions.

4.2.3 The geostrophic drag coefficient and the wind ratio

In section 2.2 we presented the basis for using the concept of drag coefficient, which is the simplest way of relating a given wind to the surface stress (Eqs. (3) and (4)).

Figure 7 represents the dependence of the geostrophic drag coefficient $C_g = (u_*/V_g)^2$ on the stability parameter h/L_* based on ISABLEX-77 data. The value of $10^3 \times C_g$ decreases from 1 under unstable conditions to 0.4 under stable conditions. For the Utö data, Joffre (1982a) found that $10^3 \times C_g$ varies between 2 and 0.4 from unstable to stable conditions, respectively.

In concordance with the findings in the previous section, since the averaged wind $\langle V \rangle$ might be less affected by observational noise, it may be preferred to V_g, and the coefficient $C_f = (u_*/\langle V \rangle)^2$ varies for the same conditions from 1 to 0.5 but with less scatter in individual values (Joffre, 1983b).

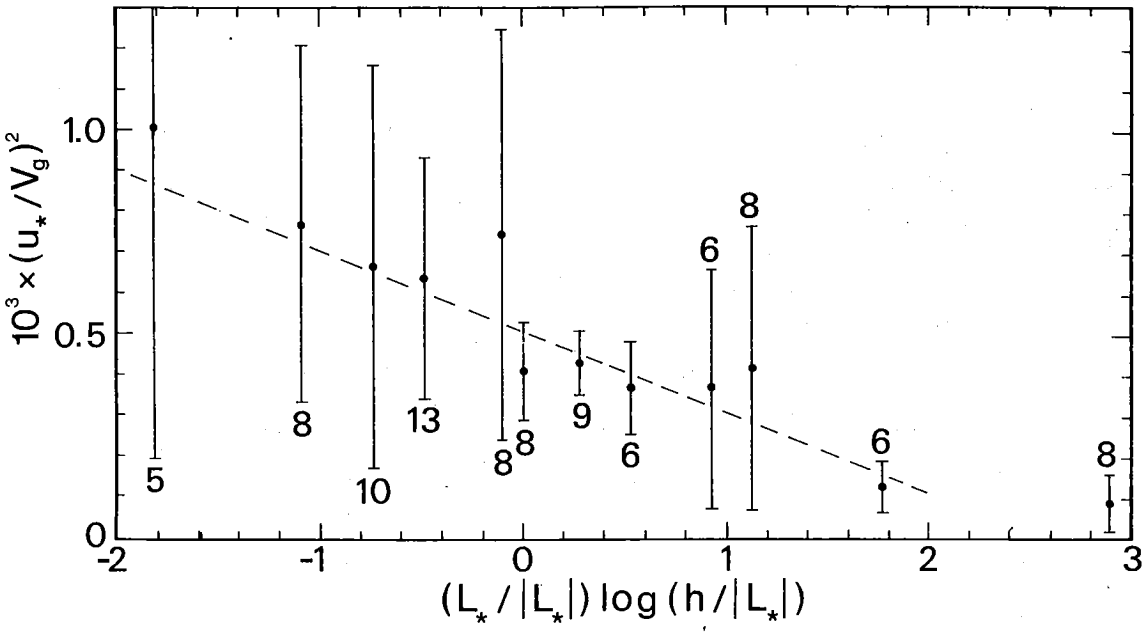

Fig. 7: Dependence of the geostrophic drag coefficient $C_g = (u_*/V_g)^2$ on thermal stability with an indication of the standard deviation and the number of observations in each mean value.

As to the wind ratio V_s/V_g, it varies between 0.8 and 0.4 for unstable and stable conditions, respectively, whereas the ratio $V_s/\langle V \rangle$ varies less for the same range of conditions, namely between 0.75 and 0.55. From the Utö data we obtained 0.78 for the ratio V_s/V_{500} under unstable conditions and 0.68 under stable conditions.

4.2.4 Effect of baroclinity and acceleration

The dependence of the drag coefficient or wind ratio on stability described in the previous section is not all. It is known, but too often ignored, that thermal wind effect (geostrophic shear) can distort ABL structure (e.g. Hoxit, 1974; Arya & Wyngaard, 1975); this too has been observed in our data (Joffre, 1982a and 1984b)

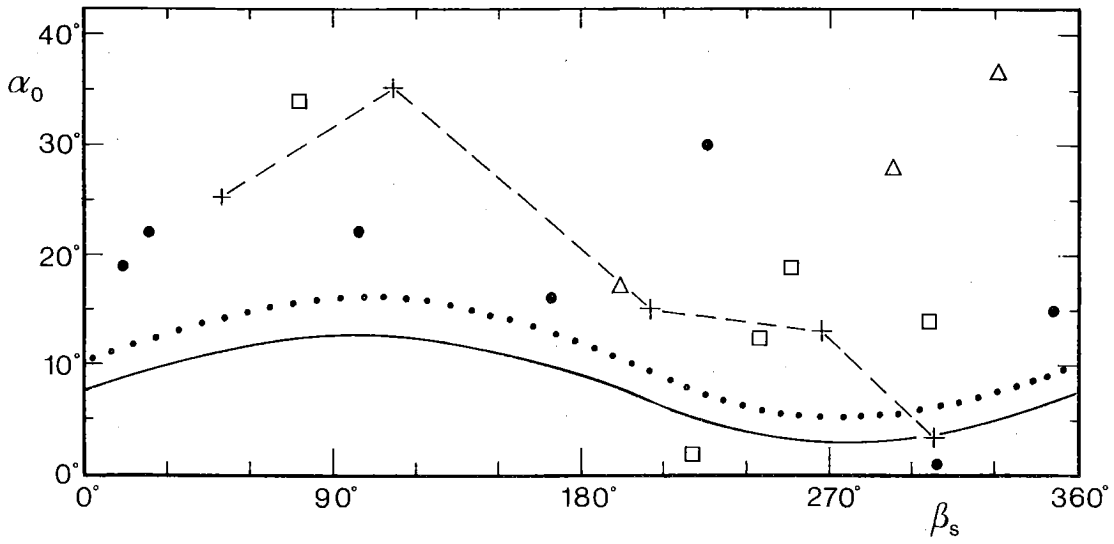

Fig. 8: Dependence of the cross-isobar angle $\alpha_o = \alpha_g - \alpha_s$ on the orientation β_s of the thermal wind with respect to the surface wind measured counter-clockwise from the latter to the direction of the former. + - - - + Isablex-77, (●) Utö ice-covered cases, (Δ) Utö stable cases, (□) Utö unstable cases. The theoretical dependence according to Arya's (1975) model is illustrated using mean ISABLEX-77 conditions (dotted line) and mean Utö-site conditions (continuous line).

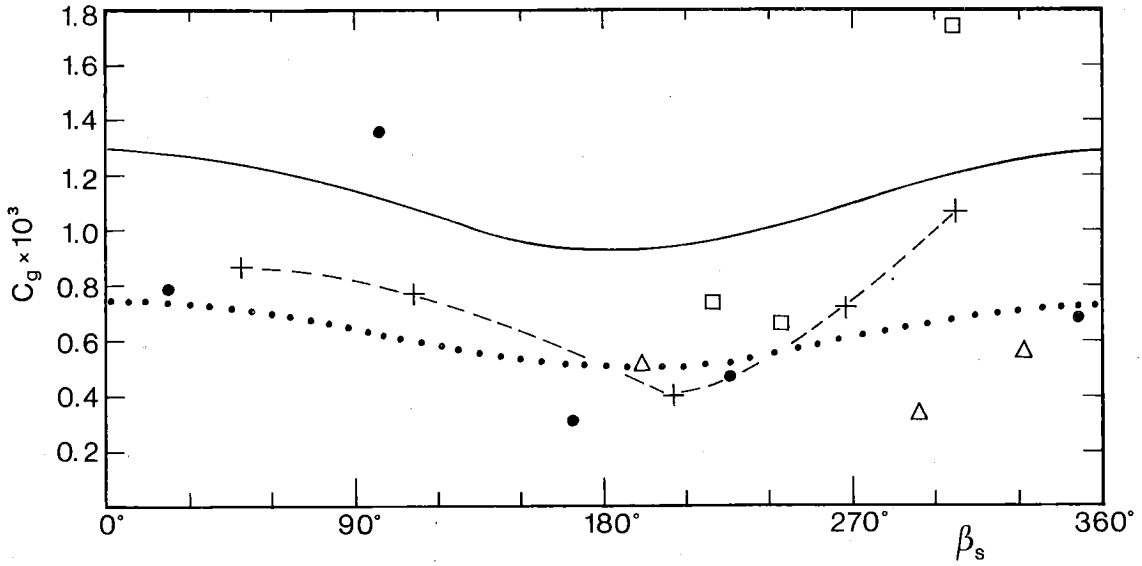

Fig. 9: Same as Fig. 8 but for the geostrophic drag coefficient.

as is illustrated in Fig. 8 . The angle β_s represents the orientation of the thermal field (isotherms) with respect to the surface wind direction. The cross-isobaric angle α_o between the isobars and the surface wind increases under cold advection conditions and decreases for warm advection. The amplitude of the effect, depending on the intensity of the thermal wind and on the parameter $\langle V \rangle / u_*$, was $\sim 20^o$ in our case. The actual wind veering, on the other hand, increases under warm advection.

The ratio V_s/V_{go} (where V_{go} is the surface geostrophic wind) is also affected but with a maximum for parallelism of isobars and isotherms and a minimum for antiparallelism (see Fig. 9). The exact position of the maximum (or minimum) can be shifted according to stability conditions .

Furthermore, inertial effects can also cause distortion of α_o and C_g. The angle α_o is the maximum for acceleration along the u-component and the minimum for deceleration along the u-component direction (v being constant). The coefficient C_g is the maximum for deceleration of the v-component (u constant) and the minimum for a time decrease in the same v-component (Fig. 10). Here, too these sine or cosine-like curves can be shifted backwards or forwards according to stability conditions and the value of the scale height ratio $h\,f/u_*$. The amplitude of the variation in α_o was $\sim 20^o$ whereas C_g doubled from acceleration to deceleration cases. The importance of the dynamical parameter $h\,f/u_*$ has been pointed out in many instances during this research (Joffre, 1981, 1982a, 1984a and 1984b) and by Arya (1975, 1977 and 1978).

Naturally, in practice it is a hopeless task to extract from observations the separate effects of stability, baroclinity and inertial effects. For the inertial effects, some conclusions have been presented by Hasse (1976), Mahrt (1974 and 1975) and Joffre (1984b). However, many observations still have to be analysed and stratified into relevant groups of external conditions so that sound statistical information can be obtained. So far, numerical modelling is the most appropriate way of computing these effects.

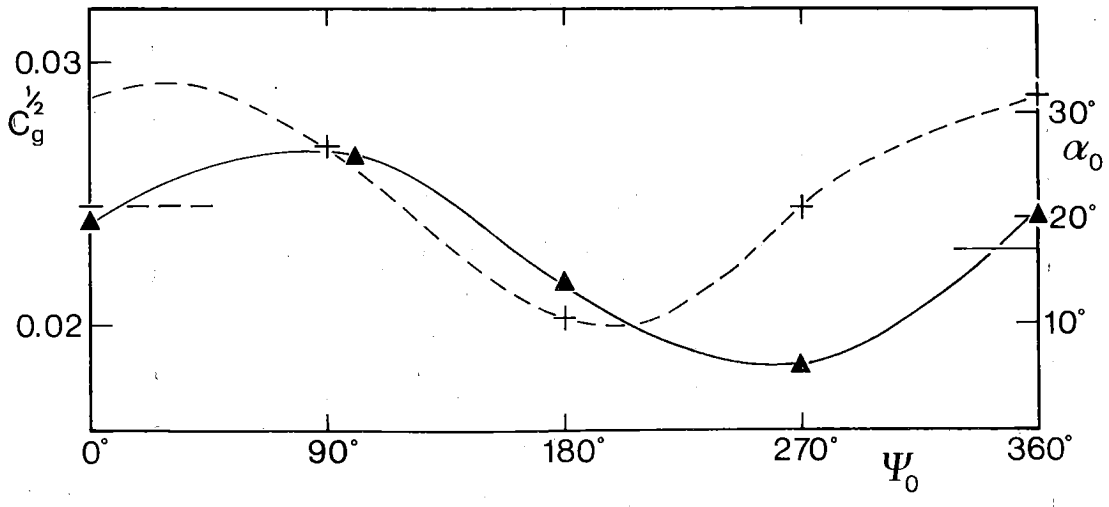

Fig. 10: Theoretical dependence according to Hasse (1976) of the root-square of the geostrophic drag coefficient (+ - - - +) and the cross-isobar angle α_o (▲——▲) on the orientation Ψ_o of the acceleration vector $(-\partial\overline{v}/\partial t\ ,\ \partial\overline{u}/\partial t)$ with respect to surface wind, taken positive for counter-clockwise rotation from the direction of the latter.

4.2.5 The evolution of the ABL height

First of all, the main difficulty with the ABL height h is determining it from profiles of mean quantities since the profiles of turbulence quantities are not generally available. It is generally believed that a more or less abrupt shift from a turbulent to a non-turbulent medium should leave in the profiles of mean quantities a trace at height h, representing the depth of the layer of active turbulence. Although this is sometimes true, it is far from being a universal rule and, what is more, fluctuations in the profiles often confuse the whole picture and subjective judgment is necessary when deciding where to set h.

Our subjective determination of h was checked by an objective one using the momentum and heat balance constraint. The turbulent fluxes were taken as the residual of the equations of motion and temperature, with h corresponding to the level where those fluxes tend towards zero. A radiative model was included in the stable

case to account for infrared cooling. The method and results have been presented in detail in Joffre (1981). Although the scatter was large, the agreement was reasonable.

Since the ABL height is seldom determined from routine observations, we are left with two alternatives for assessing h: the use of either a diagnostic or a prognostic relationship. Unfortunately, the best method available has long been a subject of debate in the literature especially for the stable case (e.g., Yu, 1978; Mahrt et al., 1982) and the problem has still not been solved. Many of these formulae contain turbulent quantities which themselves are unknowns and have to be predicted. Furthermore, the variability in these uncertain turbulent quantities can make the computed h vary much more than it does in reality. Joffre (1981) has even found that an additional scale involving the upper stratification is necessary to describe adequately the variations in h. The approach like that presented by Stull (1983a and 1983b) using bulk external parameters might be more promising.

The growth of the ABL occurs through entrainment processes at the top of the ABL. Prediction of the average wind shows that entrainment effects tended to be small in our observations (Joffre, 1984b). However, we showed that the dimensionless rate of entrainment $\tilde{u}_e = u_*^{-1} \partial h/\partial t$ in some clear situations corresponded to situations located between the laboratory results of Kantha et al. (1977) and Kato & Phillips (1969) as can be seen from Fig. 11 (Joffre, 1982c). The former corresponds to a two-fluid experiment and the latter to an initial linear stratification. Data of Kullenberg (1977) from the Baltic Sea lead to the same conclusion as shown in Garnich & Kitaigorodskii (1978). This indicates that the mechanical production of turbulence in the surface layer and in the interfacial entrainment layer at the top of the ABL is the basic ingredient during the central phase of the deepening (see Phillips, 1977; Niiler & Kraus, 1977; Kitaigorodskii, 1979 and Tennekes & Driedonks, 1981). Furthermore, Joffre (1981 and 1982c) showed that the simplified Froude number closure of Pollard et al. (1973) gave satisfactory results for modelling the time evolution of h.

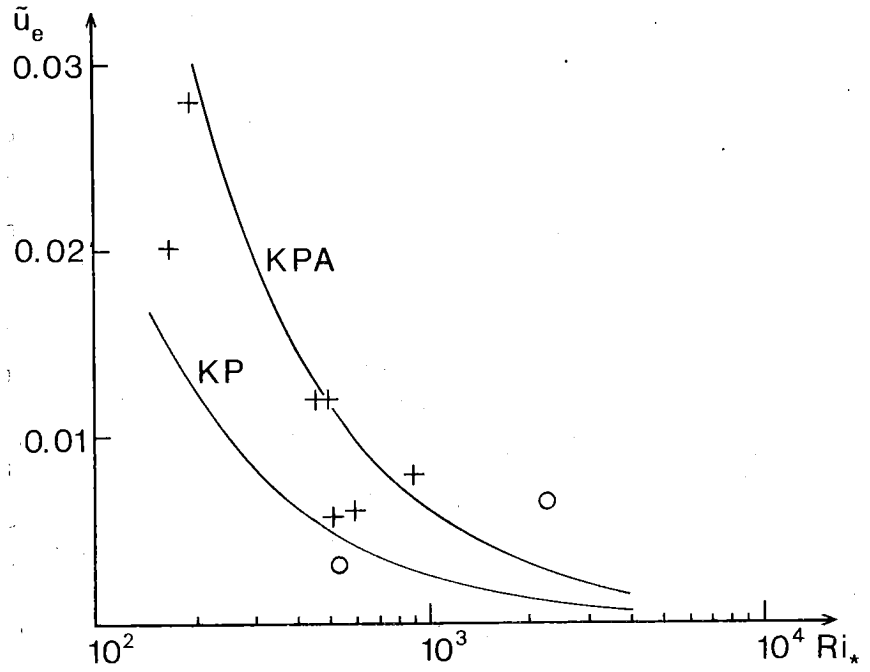

Fig. 11: Dependence of the dimensionless entrainment rate $\tilde{u}_e$ on the bulk Richardson number $Ri_* = (g/\theta_o)\, h\, \Delta\theta/u_*^2$ where $\Delta\theta$ is the interfacial temperature jump. The two curves refer to laboratory experiments of Kato-Phillips (KP) and Kantha-Phillips-Azad (KPA), respectively.

In our case of winter-time ABL over a smooth surface it may be just as good to take a constant h (or two distinct constant values for stable and unstable conditions, respectively). For instance, the average wind modelling done in Joffre (1984b) was also performed with h = 400 m and the results did not show a significant departure from what we got using the actual observed h; only under very stable conditions, was the departure noticeable. Another advantage of the 400-m level is that it corresponds on average to the standard 950-mb level. Numerical forecast models generally provide various quantities at this level.

5. STATISTICAL MODELLING

5.1 Wind statistics

Figure 12 shows the statistics of wind quantities separately for the two field experiments ISABLEX-77 and 79 where V_S is the 10-m observed wind from the mast, V_{AS} is the observed wind at 25 m at Kemi Automatic Marine Weather Station (AMWS), and W_{LW} is the estimated wind at the FMI. The idea behind the diurnal course of wind statistics is that the time of the day is correlated with stability conditions, for instance with the Richardson number Ri as it was shown with the 1977-data (see Fig. 17). However, it would have been better to stratify these statistics into, e.g., wind direction groups in order to retrieve coastal effects (Kemi AMWS is close to the coastline, ∿ 50 km). Also, Joffre (1978, his Fig. 5) showed for the Utö data that wind direction was well correlated with a local bulk Richardson number.

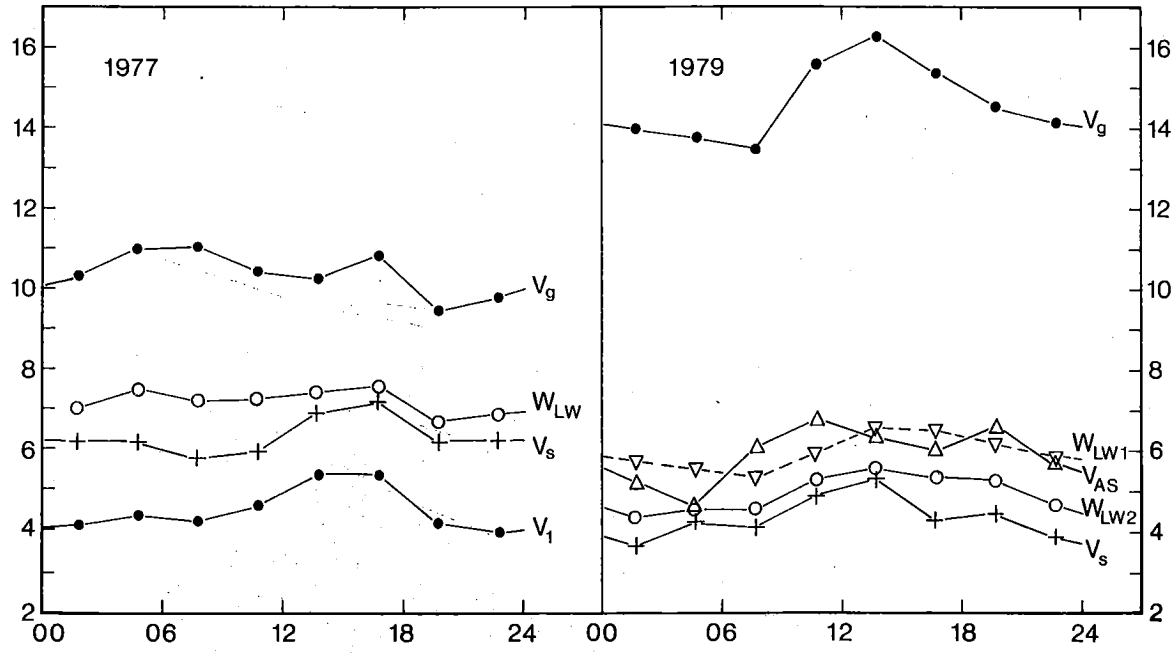

Fig. 12: Mean diurnal course of different wind velocities during the field experiments ISABLEX-77 and 79.

Note the significant difference between the two years since in 1979 the mean surface wind speed was about 2 m/s lower than in 1977. In fact, ISABLEX-77 was a good sample of real conditions for scientific work since three low-pressure systems swept over the experimental site during the period of 15 observational days. The two-peak structure in the V_{AS} curve and the weaker one in the V_s curve in 1979 suggest some kind of bidiurnal oscillation connected with a mesometeorological phenomenon or forcing such as a diurnal variation in the horizontal gradient of the temperature field or a diurnal temperature cycle over topography (Pinty & Isaka, 1982; Holton, 1967; Bonner & Paegle, 1970). In 1977, it was the computed geostrophic wind V_g that displayed a two-peak structure whereas the surface wind had a conventional diurnal cycle with a maximum in the afternoon. Thus, the two-peak structure seems to be correlated to the presence of a weaker flow. Note that over West Germany a diurnal variation in V_g of 10 % has been observed (Roth, 1981) with a maximum at 6 GMT and a minimum at 18 GMT.

The averaged 3-hourly data for the first five months of 1979 display a very smooth appearance (Fig. 13). Note that the estimated local wind W_{LW} is close to the wind data of Kemi-AMWS, since these latter are the only offshore data in the area; this is somewhat misleading since surface wind should refer to the 10-m level, whereas the V_{AS} data are from 25 m.

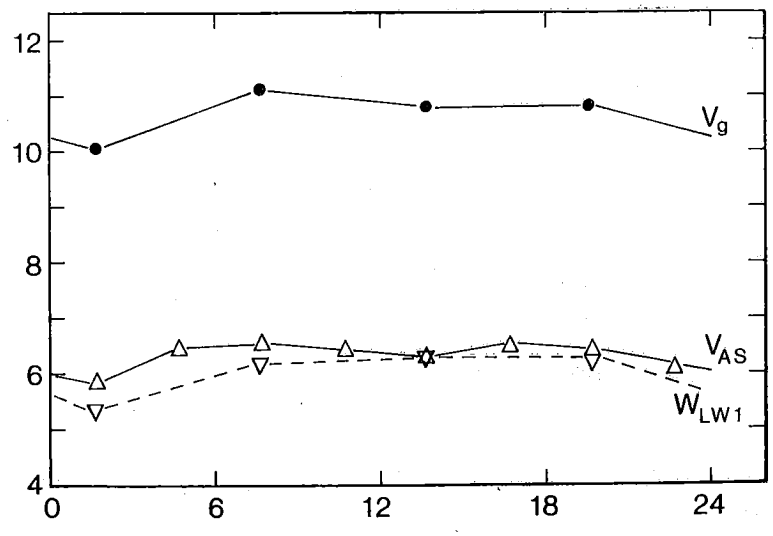

Figure 13:

Mean diurnal course of the geostrophic wind V_g, the Kemi-AMWS observed wind V_{AS} and the local wind estimate W_{LW} for sea area (1) during the period January-May 1979.

At this point we may well ask what wind information seafarers need, or whether the 10-m wind has any relevance for them. We can note that people in charge of a ship's manoeuvers coordinate operations to their own wind measurements, mostly from an anemometer along the mast at heights of 20-30 m. Consequently, wind data or prognosis should be provided to them as a quantity to which they can easily adjust mentally. Taking typical conditions ($z_o = 5\times10^{-4}$ m, implying $u_* = 0.58$ m/s from Charnock's formula) we obtain $\bar{u}(10\ m) = 14.5$ m/s, $\bar{u}(20\ m) = 15.5$ m/s and $\bar{u}(30\ m) = 16.1$ m/s. Note that this variation $\Delta u \sim 2$ m/s over 20 m vertically can be also found over horizontal distances of 20-200 km, which raises the problem of spatial representativity. Thus, the predicted wind at 10 m would be a clear underestimation in the seaman's eyes. For this reason, it is fair to calibrate wind forecasts with the wind observations at the Kemi-AMWS 25-m level. On the other hand, the screen effect of the tower with direction ranges of accelerated flow and other direction ranges of decelerated flow is no trivial matter and these effects should be studied very accurately.

Figure 14 brings yet another dimension to the complexity of the atmosphere's behaviour. It shows the intermonth variation in wind velocity at Kemi-AMWS and in geostrophic wind. Thus, it

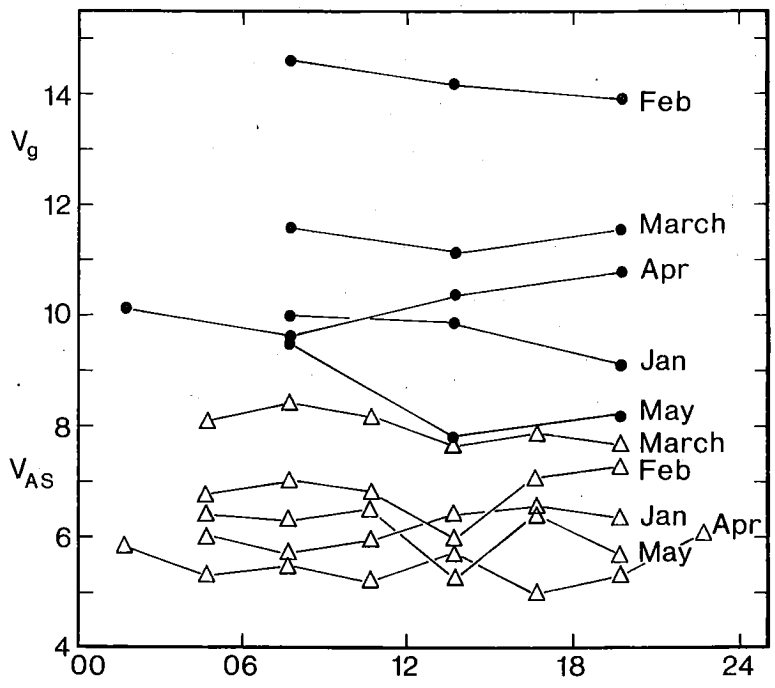

Figure 14:

Mean diurnal course of the observed wind V_{AS} at Kemi-AMWS and of the geostrophic wind V_g for the first five months of 1979.

stresses the importance of having large data bases stratified into relevant classes so that significant statistical models can be developed.

The standard deviation for predicted or observed surface winds is around 3 m/s and does not seem to depend on the time group. The fact that the estimated wind fluctuates on average in the same way as does the observed wind is a positive feature. On the other hand, the computed geostrophic wind has a larger standard deviation, about 7 m/s, i.e. 50 % of the value of the mean. The weak dependence of the average wind on the hour of the day as it appears in these figures is also an indication that other factors, e.g., wind direction, are more important. The differences between the estimated wind in area 1 (W_{LW1}) and area 2 (W_{LW2}) indicate significant mesoscale effects as observed during the JASIN-experiment (Burt et al., 1974).

5.2 Statistics of wind ratios

Figure 15 shows the different ratios computable from the wind data for the 1977 and the 1979 field experiments. For 1977 one notices that the ratio between the estimated local wind W_{LW} and the observed wind shows a peculiar peak at the morning transition. This is probably because the observed wind V_s becomes very weak at the stage of the maximum surface inversion before sunrise, but this effect is not considered in the estimated local wind. The change of the meteorologist on duty in the early morning can be also the cause for the observed discontinuity in the estimate of the wind field. Apart from this peak, which extends over three time groups, the ratio $W_{LW}/V_s \cong 1.15$, i.e. a 15 % overestimate. In 1979, the ratio W_{LW}/V_s does not display the early morning peak of 1977. Now the ratio decreases steadily from a maximum of $\sim$ 1.4 in late afternoon through the night to a minimum of $\sim$ 1.1 in early afternoon. Thus, the agreement between observed and predicted values is closest in the middle of the day with an overestimation of $\sim$ 10 %.

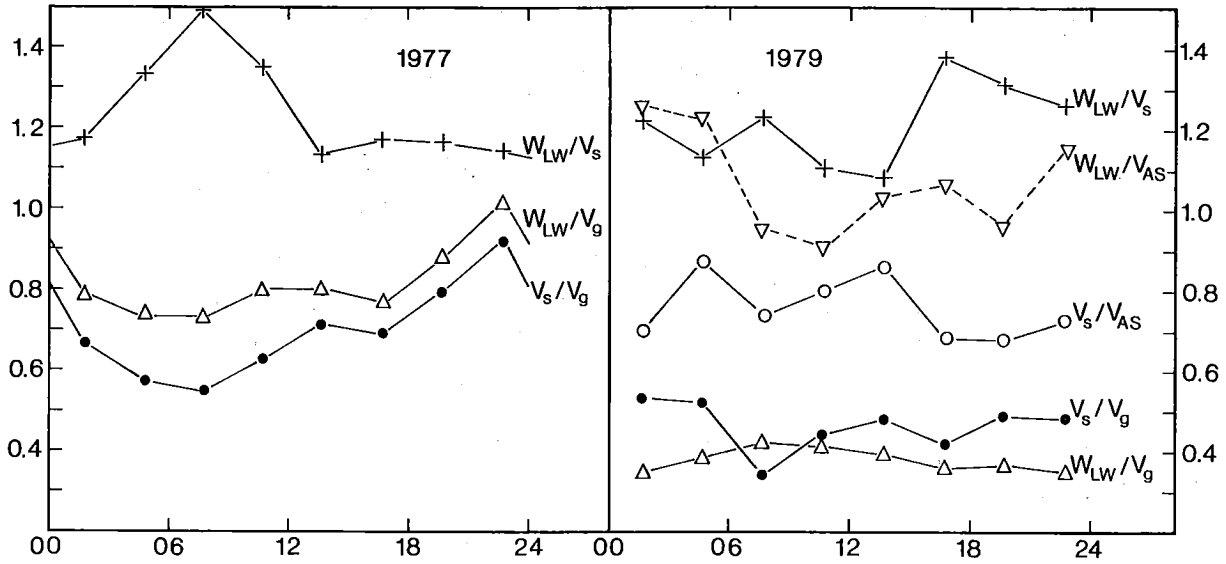

Fig. 15: Mean diurnal course of different wind ratios for ISABLEX-77 and ISABLEX-79.

One possible explanation for the sudden rise in the ratio W_{LW}/V_s in late afternoon is again the incapability of the surface analysis to cope with stable conditions. The improvement in the fit through the night may be because the meteorologist has received information and thus corrects the estimate. It is also noteworthy that this ratio has very large standard deviation values ($\sim$0.43 m/s); the real picture is therefore even less positive.

Comparison between the mast values V_s and the data from Kemi-AMWS shows that the ratio V_s/V_{AS} varies irregularly between 0.7 and 0.9. The majority of night values are around 0.7 whereas the ratio seems to increase from sunrise to 0.85 in mid-afternoon. Apart from differences on the mesoscale, the velocities differ owing to different measurement heights. Using Eq. (6) this can be expressed as

$$\frac{V_s}{V_{AS}} = \frac{\ln(10/z_o) - \Psi_{u10}}{\ln(25/z_o) - \Psi_{u25}} \qquad (16)$$

Taking typical values for the roughness of the sea surface ($z_o = 10^{-3} - 10^{-5}$ m) we obtain a ratio ranging between 0.93 and 0.91 under neutral conditions ($\Psi_u = 0$). Under unstable conditions, with $L_* = -50$ m the ratio rises to 0.96 and with $L_* = -10$ m to 0.97. Under stable conditions, on the other hand, the ratio V_s/V_{AS} is affected much strongly. For moderate inversion ($L_* = 50$ m) the ratio is 0.84 but under strong inversion conditions ($L_* = 10$ m) 0.67 . This is because increased shear implies suppressed surface wind and consequently a lower V_s/V_{AS} ratio. These numerical examples also point out the sensitivity of the results to changes in stable stratification.

The ratio V_s/V_g , which can be used as input for wind predictions, has a sine-like behaviour with a minimum of 0.55 at the morning transition and a maximum of 0.9 at the beginning of the night. Note that this is not a logical result (see e.g., Joffre, 1982a) since the ratio should have a maximum (~ 0.8) in the middle of the day because of shear. This result might be due to the difficulty of fitting the pressure field with polynomials under weak gradient conditions when the flow is not precisely defined and meanders about. From the curve V_s/V_g we see that the morning and early afternoon trend is right. This calls for the development of other techniques to enable us to compute the horizontal gradient of fields defined at grid points. A better approximation to nocturnal or winter-time anticyclonic flow might be obtained using the 850-mb field, which has to be reduced downwards. Aagaard (1969), Hasse & Wagner (1971) and Hasse (1974) presented also scatter statistics of surface to geostrophic wind relationships at sea.

The 1979 data show the same error but now the ratio is much lower owing to the large computed geostrophic wind values. Note that the ratio W_{LW}/V_g follows the ratio V_s/V_g closely. Studying the ratio W_{LW}/V_{AS} between the estimated local wind in area 1 and the observed wind at Kemi-AMWS we see that the agreement is not bad in the daytime but that the predictions overestimate the wind at night because of a deficient allowance for stability (or a biased data base). The standard deviations are very large at

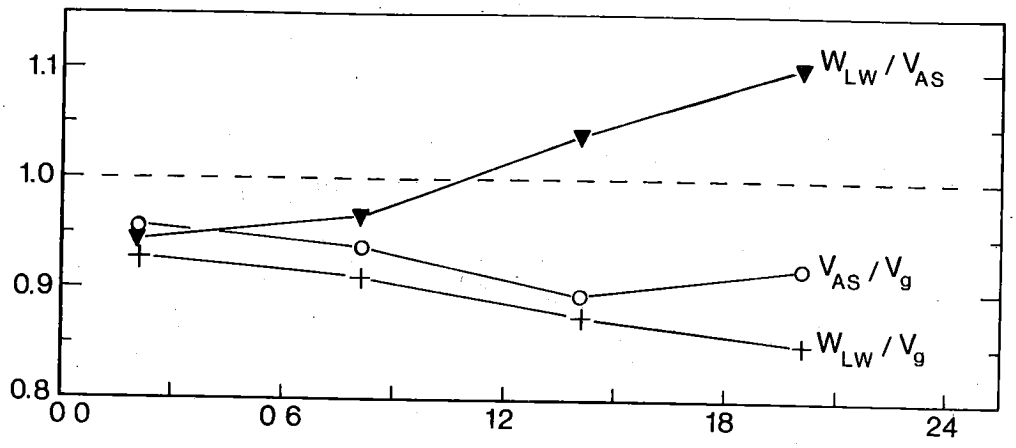

Fig. 16: Same as Fig. 15 but for the period January-May 1979.

night ($\sim$ 0.48 m/s) but moderate in the daytime ($\sim$ 0.20 m/s).

Turning now to the mean ratio for the period January-May 1979 shown in Fig. 16, we note that $W_{LW}/V_{AS} \cong 1.1$ at the beginning of the night but falls to a value of 0.95 later in the night. Thus, the local wind estimate W_{LW} is systematically too strong under stable conditions. As to the ratios V_{AS}/V_g and W_{LW}/V_g, they both seem to be too high ($\sim$ 0.85-0.95) since the ratio between surface and geostrophic wind is typically 0.8 under unstable conditions and 0.6 under stable conditions. Such ratio values would mean that V_{AS} is also too high, possibly because of an accelerated flow around the lighthouse tower. If this effect is real, it should be carefully investigated and retrieved from the data before the automatic station data can be used appropriately (see Blanc, 1983; Kahma & Leppäranta, 1981; Wucknitz, 1980).

5.3 Statistics of wind direction

We compute the differences between the various wind concept directions. In 1977, the computed geostrophic wind direction α_g compared with the observed wind α_s at the experimental site from the mast shows a typical diurnal cycle well correlated with the course of the Richardson number also computed from mast measurements (Fig. 17).

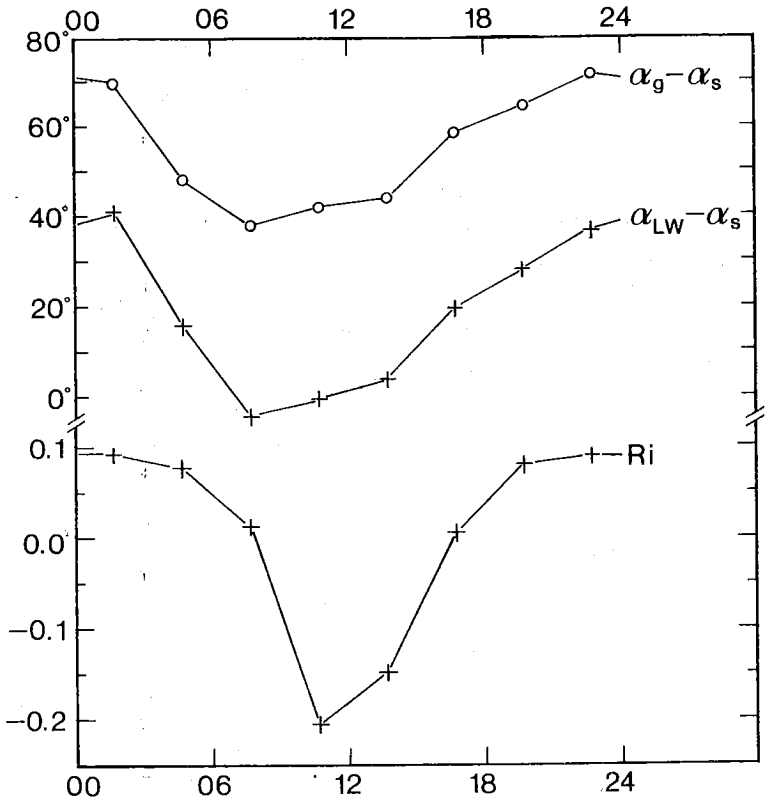

Figure 17:

Mean diurnal course of wind direction differences for ISABLEX-77 with the course of the Richardson number Ri.

The cross-isobaric angle $\alpha_o = \alpha_g - \alpha_s$ had a minimum in the daytime ($\sim 40^o$) and a maximum at night ($\sim 70^o$). Although this trend is qualitatively right, the numerical values are very large and indicate some systematic behaviour in the computed geostrophic field (either erroneous or maybe due to cold air advection). The deviation in the predicted local wind direction α_{LW} from the FMI from the observed direction α_s displays the same diurnal trend. The deviation is now close to zero for the three time groups in the middle of the day, but it increases by up to 40^o at night. This also indicates a systematic underestimation of wind turning under strongly stratified conditions and/or a biased data base together with the fact that the flow field is often badly defined at night.

In 1979, most of the wind direction deviations had a minimum in the daytime ($\pm 10^o$) and increases at night (Fig. 18), again stressing the problem connected with the night-time flow. For example, since $\alpha_{AS} - \alpha_s$ is smaller during the day than at night, this means that there are smaller diurnal differences in the flow

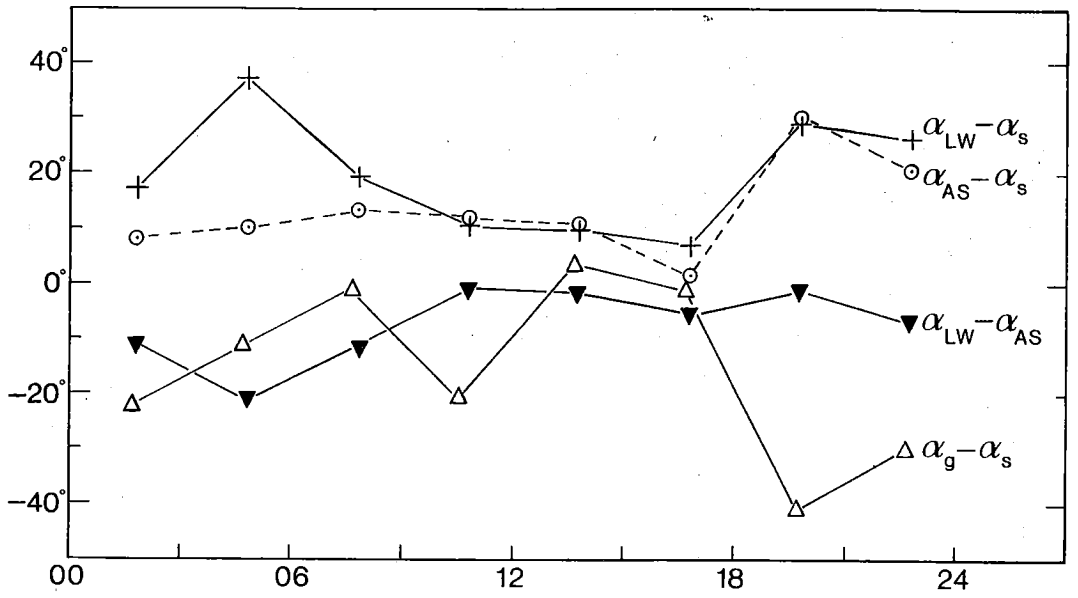

Fig. 18: Same as Fig. 17 but for ISABLEX-79.

on the mesoscale than there are at night. In consequence, forecast on a small gridmesh should be easier for daytime conditions. Here again the standard deviations in the differences were tremendous ($\sim \pm 100^{\circ}$). Note also that the cross-isobar angle shows a backing due to either the above difficulties with the V_g vector computations or peculiar baroclinic conditions.

Taking the mean for the first five months of 1979 gives large variations in the deviations $\alpha_{AS} - \alpha_g$ and $\alpha_{LW} - \alpha_g$ whereas $\alpha_{LW} - \alpha_{AS}$ is rather constant ($\sim -10^{\circ}$) all day, confirming the calibration of local wind estimates on the Kemi data (Fig. 19). Note that the difference $(\alpha_{LW} - \alpha_g)$ generally contains more data than the two other differences, thus, explaining the phase shift between $\alpha_{LW} - \alpha_g$ and $\alpha_{AS} - \alpha_g$ although the angle $\alpha_{LW} - \alpha_{AS}$ is practically constant.

It can be noted that $\alpha_{LW} - \alpha_g$ and $\alpha_{AS} - \alpha_g$ change sign during their diurnal cycle so that if day day averages were taken the overall mean difference would be closer to zero, thus implying a fair agreement. The difference $\alpha_{LW} - \alpha_g$ could be fitted by a cosine-function and $\alpha_{AS} - \alpha_g$ by a sine-function. Thus, there is a $\pi/2$-phase shift between them.

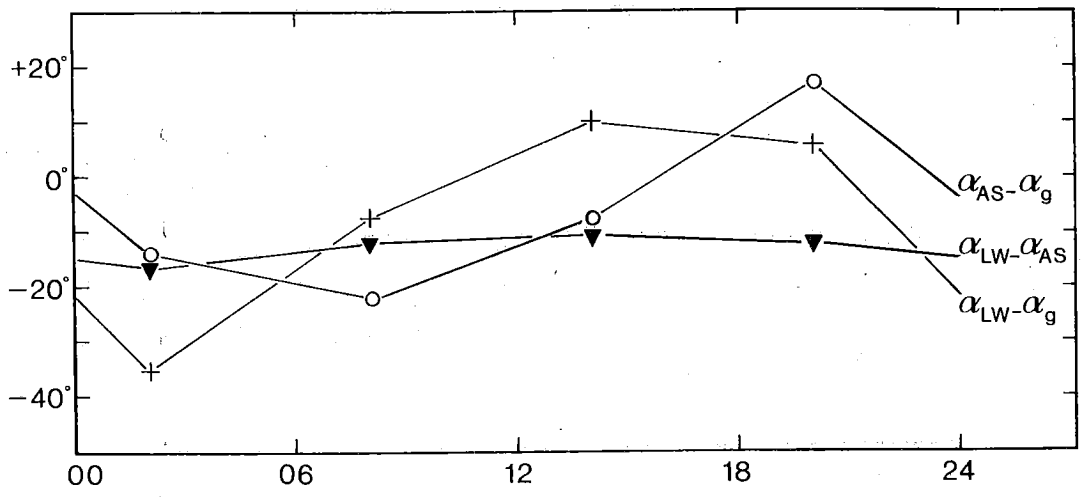

Fig. 19: Same as Fig. 17 but for the period January-May 1979.

6. SURFACE WIND MODELLING

6.1 Background of the model

Accurate simulation of surface processes over sea areas requires knowledge of the atmospheric inputs (momentum, heat and mass) in connection with weather variations. Here we are basically concerned with the simulation of the surface stress, and we can model it in three ways:

- a) direct simulation within an ABL model (e.g., Brown & Liu, 1982; Busch et al., 1976);
- b) by connecting it to the near-surface flow (lowest grid point or surface wind V_s), e.g., Pease et al. (1983), Macklin (1983);
- c) by connecting it to the upper flow (V_g , V(h) , <V> , V(900 mb) or V(850 mb)), e.g., Feldman et al. (1979 and 1981), Kau et al. (1982).

Method (a) would require us to solve the Navier-Stokes equations at the grid points. The complexity of a turbulence model implies that its outputs are at the same level of accuracy as its inputs. This is not fulfilled for average mean winds over

large areas. Furthermore, it requires various input data or boundary conditions which are generally beyond our grasp on the routine level.

The simplest approach of a statistical model (as in (b) and (c)) using one or more suitable predictors explaining, let us hope, most of the variations in the considered parameter might then be more relevant in certain cases. Better accuracy could obviously be achieved by considering several predictors, but it is not always easy to extract the isolated influences of each parameter from data sets. On the basis of the previous results we choose the quantity $\langle V_{400} \rangle$ as the main predictor for the surface wind since it is closely related to V_g (see Joffre, 1983b, Fig. 8), the main external driving force, and it is little affected by stability (Fig. 20). In this figure, there are some points corresponding to strong $\langle V_{400} \rangle$ which do not follow the smooth increasing trend observed at lower speed. These points correspond to some transitional neutral cases and to uncertain stable cases;

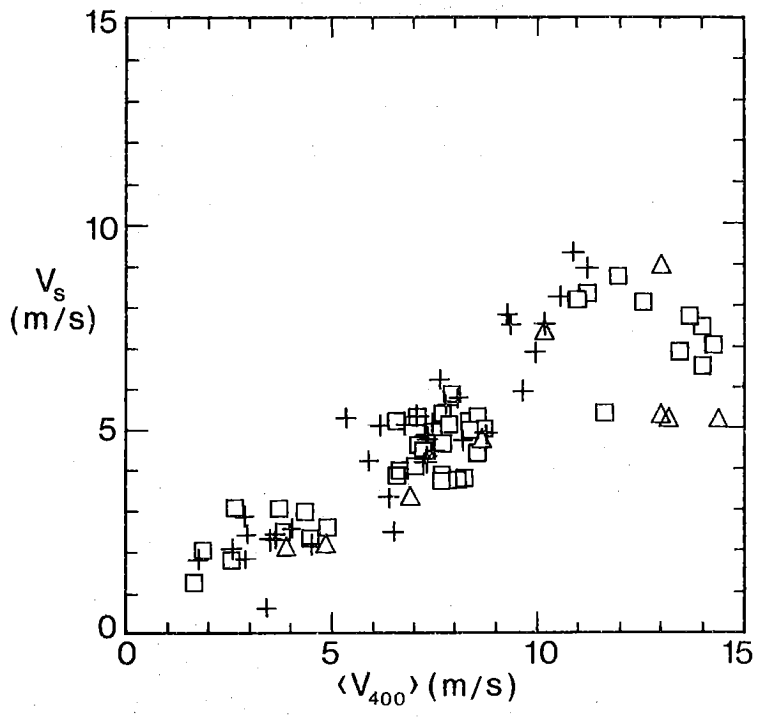

Fig. 20: Scatter diagram between the observed surface wind V_s during ISABLEX-77 and the vertically averaged wind $\langle V_{400} \rangle$. (Δ) near-neutral, (□) stable and (+) unstable cases.

these few points are not included in the linear regression fit. We note also that while the trend between V_s and $\langle V_{400} \rangle$ is linear for bulk velocity less than 7-8 m/s, the trend seems to increase with velocity at higher bulk velocity. However, we lack high velocity wind observations, and the consequences of this will be observed in the next section.

The surface wind direction is determined using the ABL mean wind direction α_m defined as (with $V = (u^2 + v^2)^{\frac{1}{2}}$) :

$$\alpha_m = \tan^{-1}(\langle v_{400} \rangle / \langle u_{400} \rangle) \qquad (17)$$

This bulk cross-isobaric angle is weighted statistically using the observed values.

V_s still has to be related to the surface stress and this is strongly dependent on thermal stability. One way round this problem is to lower the reference level to, say, ca. 1 m, so that we are always within the dynamical sublayer where buoyancy effects are not important. We already know that a well-defined linear relationship exists between the stress and this low-level wind V_1 (see Fig. 4). Furthermore, the ratio $V_1/\langle V_{400} \rangle$ is well defined (showing small scatter) and depends smoothly on stability (Fig. 21). Note that this minimum wind V_1 is not intended for practical purposes (since it has no real meaning above, for instance, a rough wavy sea surface) but as an intermediate tool for forecasting purposes.

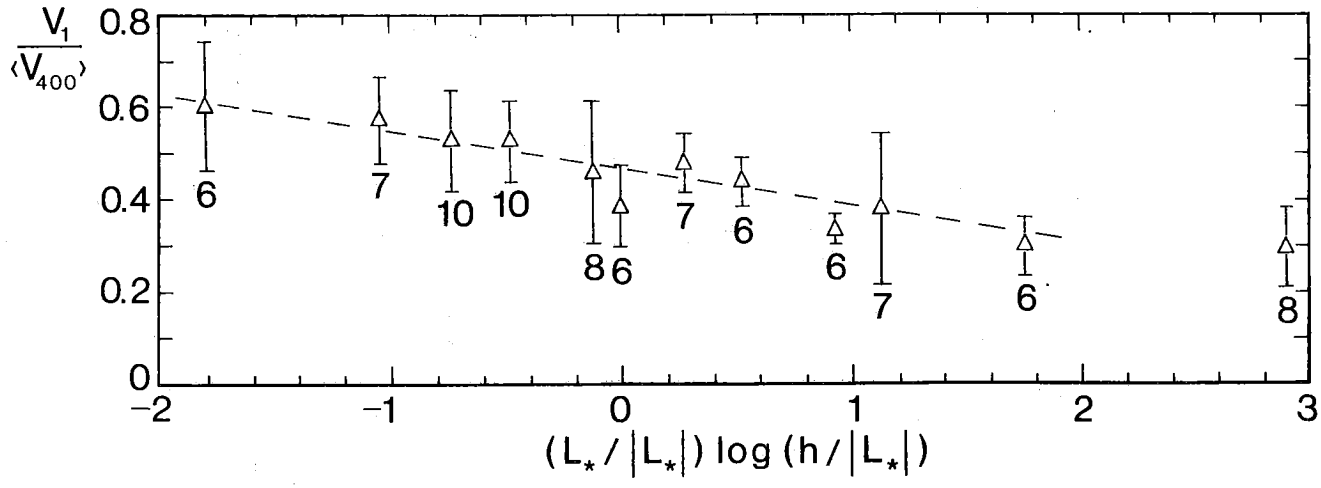

Fig. 21: Dependence of the ratio $V_1/\langle V_{400} \rangle$ on thermal stability h/L_*. The figures refer to the number of observations included in each stability group.

Table 3 shows the variation in the linear regression coefficients between the surface wind V_s and the geostrophic wind V_g and between the observed wind direction α_s and the geostrophic wind direction α_g for the eight time groups (00.30-03.00 , 03.30-06.00 , etc.). Thus, a model based only on V_g should include a stability dependence whereas <V> was independent of stability (fig. 20).

	V_s vs. V_g			α_s vs. α_g			
Group	r	a	b	r	a	b	$\overline{Ri}$
1	.88	.461	1.45	.80	.897	-61.8	.093
2	.87	.509	0.59	.79	.782	-33.0	.084
3	.82	.502	0.35	.94	.894	-27.0	.026
4	.82	.539	0.10	.97	.868	-30.9	-.168
5	.89	.645	0.15	.97	.850	-31.3	-.182
6	.87	.739	-0.83	.97	.981	-53.8	-.008
7	.79	.513	1.34	.98	1.213	-85.2	.079
8	.81	.430	2.09	.93	1.154	-81.9	.088

Table 3: Values of the coefficients in the regressions $V_s = a\,V_g + b$ and $\alpha_s = a\,\alpha_g + b$, with r the correlation coefficient. $\overline{Ri}$ is the average Richardson number for each group based on mast measurements. Only cases with $V_s > 2$ m/s are included in this Table.

6.2 Results

Using the 1977 profile data base (observations at irregular times and only between 6 a.m. and 9 p.m.), we can simulate the course of the surface wind at synoptic hours during the March-April 1977 period. Thus, although individual test data are dif-

ferent from the calibration data, they belong to the same weather patterns. These results are compared with the local wind estimates W_{LW} made at the FMI. These wind estimates are also used at the FMI as input data for a statistical model (Lange, 1973) based on prediction from a numerical forecast model with correction from wind statistics to allow for diurnal, seasonal, orographic and mesoscale factors. It is basically a regression model based on a small data base. The basic flow is modified by only a few Fourier harmonics; effects such as stability and baroclinity are not explicitly accounted for. Finally, before they are released to the users, the numerical local forecasts are corrected subjectively by the meteorologists on duty. Forecasts are given every six hours up to 36 hours for eight sea areas (see Fig. 2).

Our model, on the other hand, tries to account implicitly better for physical effects such as diabatic forcing and disturbing effects such as baroclinity and inertial acceleration, which are taken as small perturbations on the basic state. It is not a time-dependent method and thus it requires knowledge of the predicted large-scale flow.

The results are shown in Figs. 22 and 23 for the two experimental sites, respectively. We define the fractional error σ_V as

$$\sigma_V = 100 \frac{V_{prd} - V_{obs}}{\frac{1}{2}(V_{prd} + V_{obs})} \qquad (18)$$

in order to test the agreement between the predicted wind V_{prd} and the observed wind V_{obs} on the mast. As it appears in the Figures our bulk model gives better results with $\sigma_V = (-19.5 \pm 27)\%$ in March and $\sigma_V = (-2.1 \pm 25)\%$ in APril. The FMI estimate W_{LW} yields $\sigma_V = (23.5 \pm 43)\%$ and $(9.2 \pm 28)\%$ in March and April, respectively. Moreover, the smaller standard deviations in the bulk model indicate that, on average, erroneous forecasts are less serious than when using the FMI estimate. The positive sign of σ_V for the local winds indicates that it overestimates observed 10-m winds (see § 5.1), although it may underestimate ship's wind recordings from the mast top. The negative values of σ_V

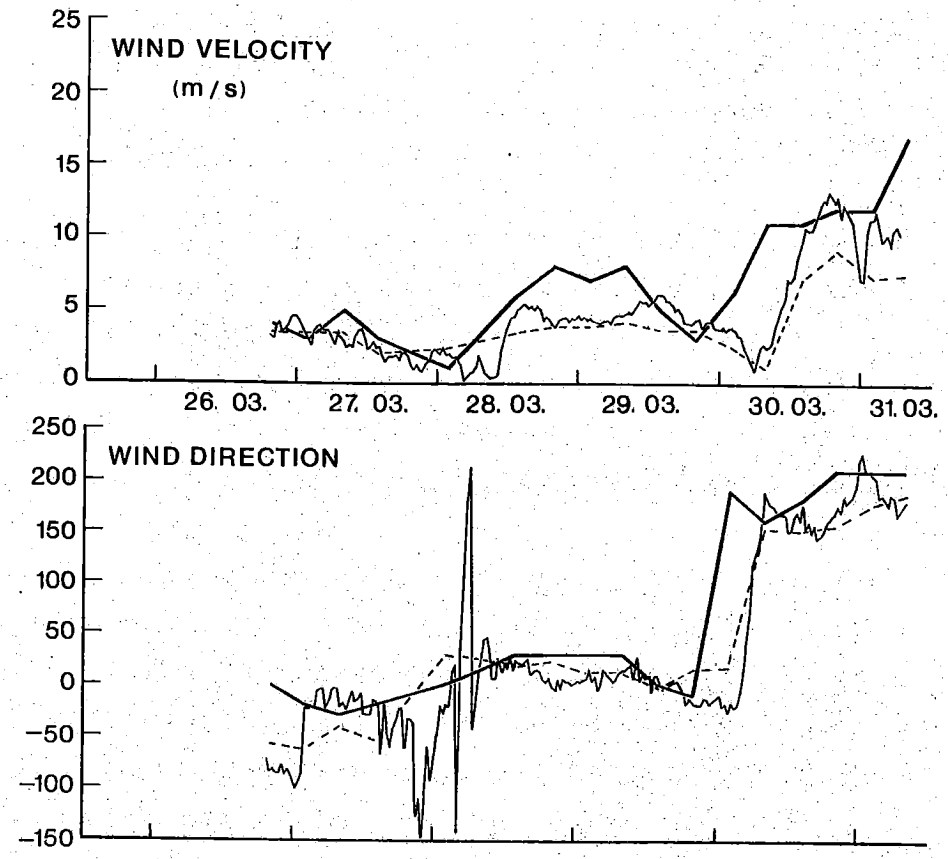

Fig. 22: Comparison of the FMI local wind estimate (Thick continuous line) and our bulk statistical forecast (dashed line) with observed 10-m wind at site 1 during ISABLEX-77.

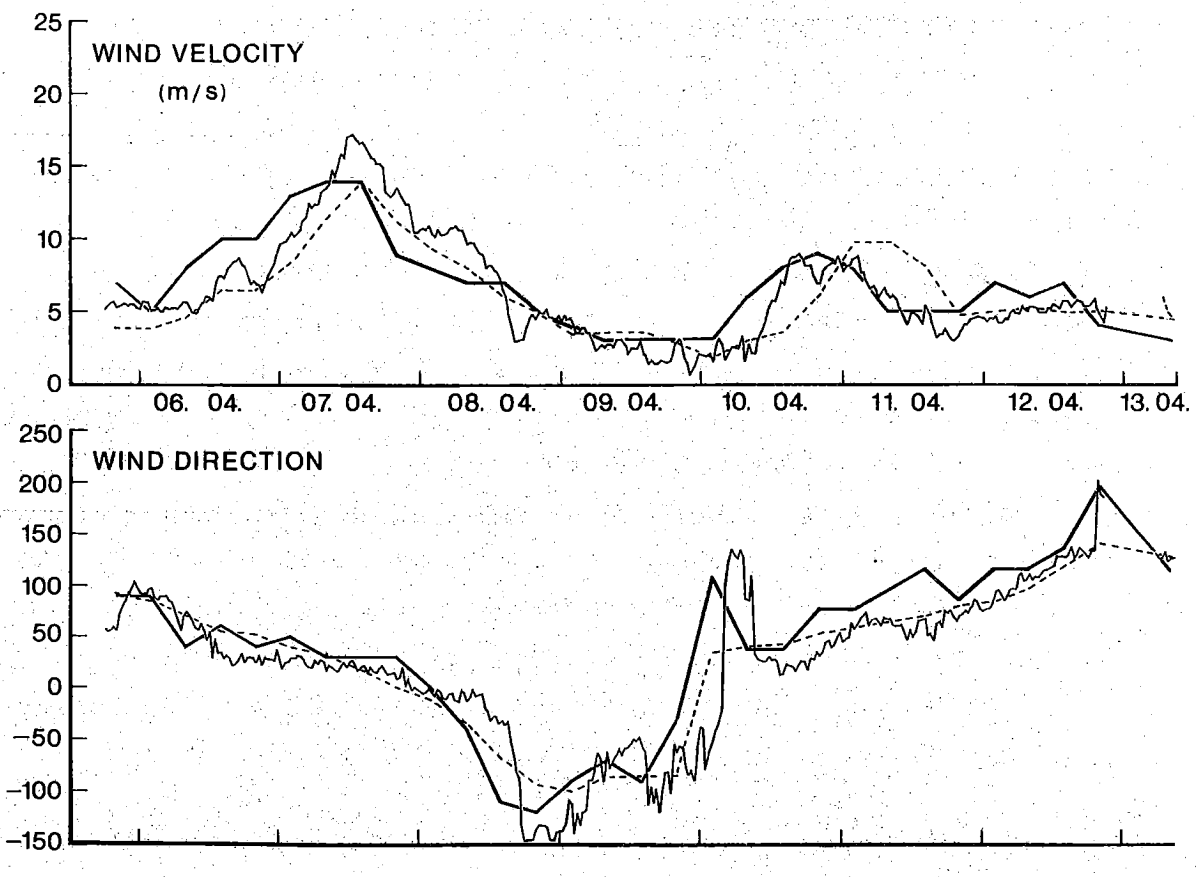

Fig. 23: Same as Fig. 22 but for site 2 of Isablex-77.

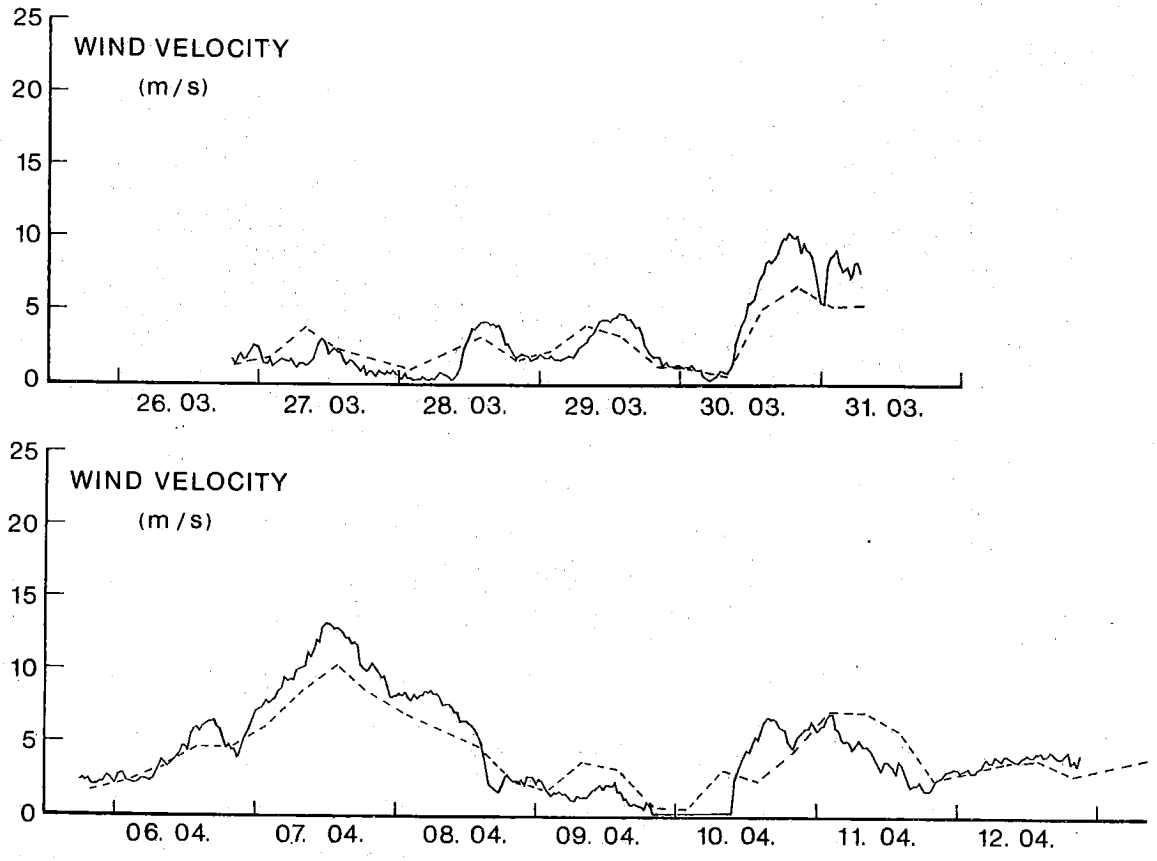

Fig. 24: Comparison of predicted 1-m wind with the bulk model (dashed line) with observed 1-m wind velocity during ISABLEX-77.

(underestimation) of our bulk model are partly due to the fact that the data base did not contain strong wind cases owing to the difficulty of observational work under these conditions. This calls for more data especially during stormy weather (ISABLEX-79 was of no help in this respect).

Figure 24 shows the prevision for the V_1 wind; the agreement appears to be quite satisfactory.

ISABLEX-79 was so unusual with many uncertain weak winds and a peculiar, very strong computed geostrophic wind that comparison with observations was meaningless. Fitting a simple linear regression between V_g and V_s for the 1979 data (N = 32) gives $V_s = 0.172\ V_g + 1.85$ and a correlation of 0.38. For the ISABLEX-77 data (N = 47) the same fit gave $V_s = 0.524\ V_g + 0.85$ and a

correlation of 0.82 . These results clearly show the distinct flow conditions during the two experiments.

A noteworthy feature is the forward shift noticeable at the start of unsteady periods in the local wind W_{LW} together with the geostrophic wind with respect to observations. The increase in wind or the change in wind direction are by and large predicted to start about 6-9 hours before they are observed. This may be attributted to a sampling error during the geostrophic wind calculation procedure, which takes grid points 2×150 km apart to compute the pressure gradient; thus, in rapidly changing situations each grid point does not reflect the same flow pattern. This effect was empirically corrected in our bulk model (see Joffre, 1983b). This effect stresses the importance of numerical field analysis and of recognizing that unwanted artificial features can be introduced via the analysis.

The results of the method are encouraging enough to incorporate additional observation data in the statistical regression and thus to extend the applicability of the method. On the other hand, the difficulty associated with the geostrophic wind, especially under stable conditions, calls for an alternative method involving, for instance, the upper level driving flow, e.g. the 900- or 850-mb wind or the 850-mb geostrophic wind or the output wind from a numerical forecast model like that of the ECMWF (European Centre for Medium Range Weather Forecasts). We have compared here the wind analysis estimates of the FMI to real offshore data, however, it would be enlightning to compare these observations to the actual predictions of Lange's (1973) model.

7. RECOMMENDATIONS AND CONCLUSIONS

7.1 Potential modelling algorithms

Now we turn to the problem of possible operational routines providing necessary inputs to oceanographic models (e.g., ice-drift model, water-level models). It is to be noted that, for historical reasons, different models needs different inputs (Rinne et al., 1984) although they all need the surface stress in the end. Moreover, although meteorological data are computed over large domains ($\sim$ 150 km), oceanographic models use a much finer gridmesh ($\sim$ 30 km). Thus, it is necessary to incorporate different reduction routines. They can be grossly divided into two main groups: models requiring either surface inputs or upper-layer inputs (see Table 4).

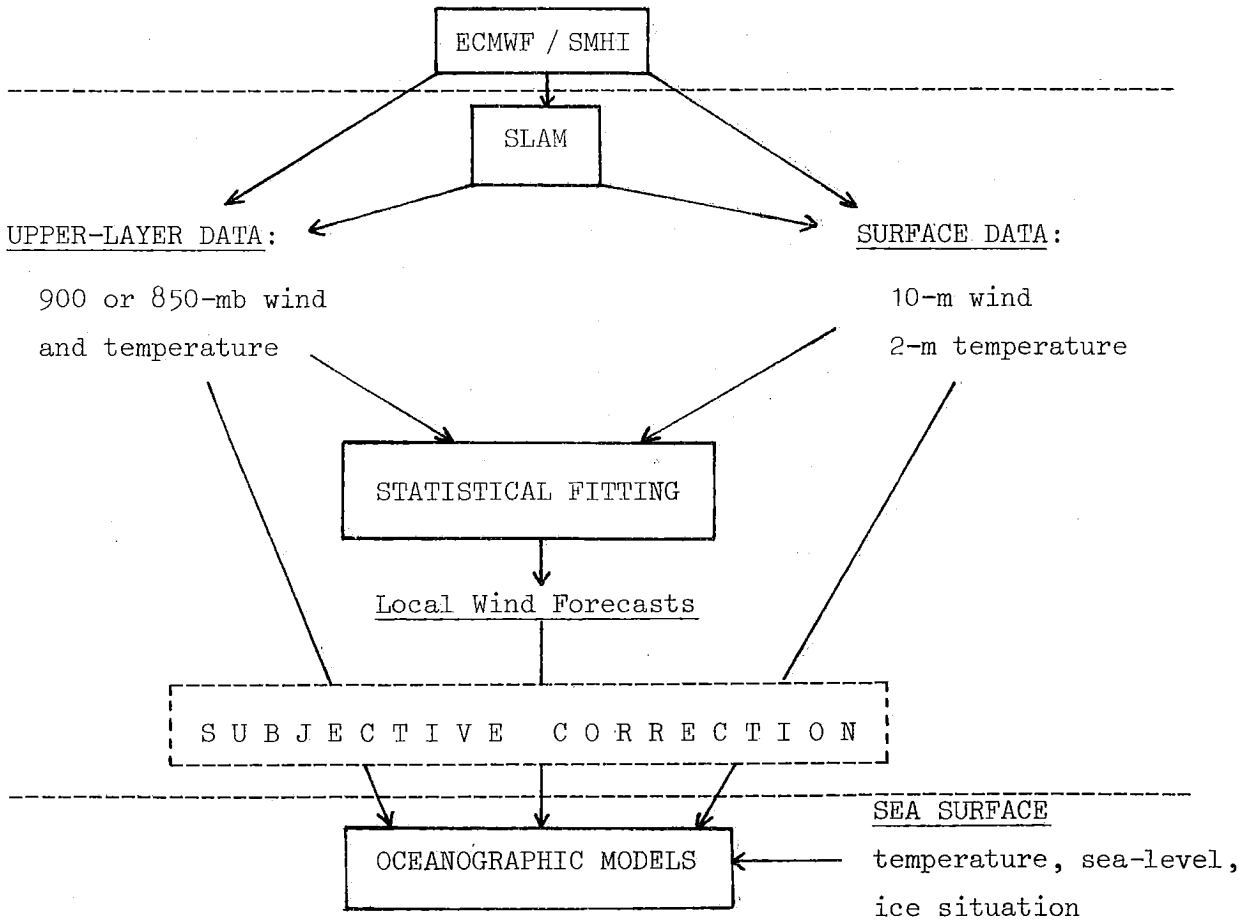

Table 4: Flow chart of possible data transfer and modification from Direct Model Outputs towards surface wind predictions.

Obviously, a third way would be to provide the stress or u_* directly but, at the present stage, meteorological models do not have such output.

- a) surface inputs:

The ECMWF and SMHI models can furnish temperature and wind forecasts close to the surface (2 m and 10 m, respectively) on a grid ($\Delta x = 150$ km). These are called Direct Model Outputs (DMO) and they describe large-scale flow conditions so that they should be corrected statistically to fit real local conditions. Moreover, the interpolation for sea areas uses land grid points as well, and thus a suitable weighting procedure should be incorporated.

The statistical calibration can be performed in three different ways (Table 5). Note that the problem in alternative (3) is the small number of observing stations and the interpolation to a small grid, especially close to the coast where conditions change drastically over a short distance. On the other hand, alternative (3) is easier to perform because the required observational data base is available.

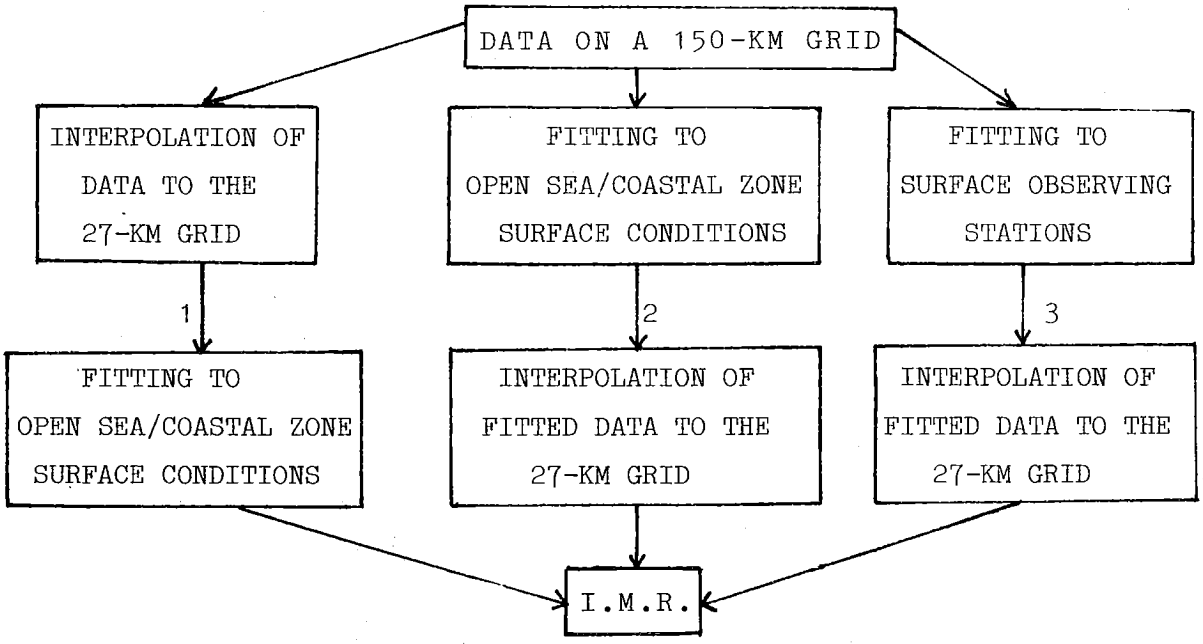

Table 5: Possible statistical interpretation schemes of DMOs towards surface forecasts on a fine grid.

- b) upper-layer data:

Temperature and wind (geostrophic or actual) forecasts on a 150-km grid can be obtained from various numerical models at 1000, 900 or 850 mb. These data can also be reduced statistically to surface quantities by statistical methods.

There are two main methods of statistical interpretation for reducing the model outputs. One can use older observational material of concomitant upper and surface data to be applied to numerical forecasts (Perfect Prog technique) with the assumption that forecast upper data are exact. This is the method applied in section 6. Or one can use a data base consisting of previous forecast upper data. This method can eliminate the systematic errors of the numerical forecast model but it has the major drawback that the available material generally covers a short period. Both techniques are based on regression analysis including several predictors.

It is evident that the ECMWF model, by the time the Limited Area Model (SLAM) of the FMI has shown its capability, has the potential to match a great number of different situations because of its complexity and extensive computational background. The recently opened direct link between the FMI and IMR computers now permits trouble-free transfer of data. Note that the ECMWF model is aimed at medium-range forecasting; short-term forecasts may therefore be hampered by an initial lag of $\sim$14 hrs in data assimilation, but this is only likely to be serious during rare, rapidly changing situations. Then, the SLAM of the FMI may give better results by using newer input data. This danger could be avoided with a routine comparing the first forecast field at 00Z with the new analysed field of the FMI or by comparing only the forecast surface wind with the statistically regressed surface wind using the most recent pressure or wind field.

The ECMWF forecasts are currently available on a 150-km grid in table or vector representation. The present scheme at the FMI interpolates them to the centre of four sea areas covering the Bothnian Bay and the Bothnian Sea. The first comparisons performed at the FMI (Kukkonen, 1982) show that these predictions

are fair. However, the comparisons were not performed against real observations, since they are lacking over open sea areas. Moreover, the test consisted of only a short summer period. This stresses the importance of having automatic maritime weather stations functioning all year round.

If one assumes that we have reliable meteorological data on a 150-km grid, it appears that the crucial step is the interpolation down to a local scale. Here we have only used a second-order polynomial technique. Third-order polynomial techniques might not give better results since the procedure requires more outermost data and in the case of the Bothnian Bay, this means more continental data to determine pressure gradients at a sea site. A fundamental drawback of polynomials is that meteorological fields do not follow polynomial distributions. A more appropriate method might be the bicubic polynomial splines dividing the grid size into 8 subintervals as successfully used for water level predictions by Häkkinen (1980). A more exact description of the wind field is necessary under rapidly changing conditions, although this is smoothed out during the 6-hours intervals between pressure field analysis at the FMI and for complicated flow patterns.

7.2 Further work

The theoretical work carried out during this investigation improving our understanding of some of the processes involved in the transfer of momentum from the atmosphere to the sea surface has cleared up certain issues and provided numerical estimates of certain parameters necessary for surface stress modelling. This stage can be considered to represent the end of the basic research since similar additional investigations will not bring much more information owing to the stochastic nature of turbulent processes and the large empirical noise present in observations. We have already started a second phase of research aiming at acquiring statistical knowledge of the relationships

between different meteorological quantities. We have managed to extract a representative predictor <V> and reject another one, the geostrophic wind. However, these studies have been carried out with a small data base from a special observation campaign. Implementation for statistical purposes requires many years'data and for this purpose the only data bank is that at the FMI. One strategic issue is to define appropriate and physically representative data groups by properly and judiciously stratifying the data base on at least two levels (e.g. groups according to wind direction and these further into time of the day groups); note that grouping in the opposite order would lead to different results. On the other hand, these long series of routine data do not contain all the details of external and internal parameters included in field experiment data. Consequently, these two sources of information should be combined and the work continued where the data banks are,by scientists skillful in data processing and numerical analysis. Especially statistical calibration of ECMWF forecasts with surface observations should be pursued and encouraged.

In any case, the first and perhaps the most important step is to decide the source and type of basic wind input. We saw that in many instances the geostrophic wind presents certain theoretical and especially observational drawbacks. Joffre (1984b) shows that any observed wind concepts are a better estimate than V_g since we avoid the problem of relaxation of the non-divergent homogeneous geostrophic flow towards the actual flow field. Thus, the balanced wind at 900 or 850 mb from either the ECMWF or the Finnish SLAM model may constitute a better starting point. This is particularly true under stable stratification conditions (night situations or winter-time anticyclonic situations) when the geostrophic wind is hardly computable from the undefined pressure field.

The next step would then be to relate this upper wind to surface values, taking into account various stability, baroclinity, roughness and acceleration conditions. Since these 10-m wind forecasts are available from a sophisticated global numer-

ical model, all the parameters required for assessing factors (time changes, horizontal gradients of temperature and/or wind) perturbing the concept of a constant drag coefficient are available or computable directly from the model, thus permitting a great deal of complexity.

However, in order to have adequate products, correction and interpolation are also necessary on a local base, along the lines mentioned above, the final purpose being to differentiate these statistics on the mesoscale in order to take regional differences into account. The data from the AMWSs could be very valuable at this phase. Likewise, the reliability of these AMWS data should be investigated since the flow can be distorted by the bulk structure of the lighthouse and their representativeness altered by the vicinity of the coast for offshore wind conditions. This type of fine testing of routine observations should be extended to all coastal stations in order to estimate local distortion of the flow (by nearby trees, houses, etc.) and the influence of the coastline on the observations on the meso-γ scale.

Note also that ECMWF outputs or AMWS data could be used to refine our bulk model by allowing direct assessment of stability conditions since the model provides the 2-m level temperature and the AMWS data provide surface layer air temperature and water surface temperature. In the case of ice-covered sea, only some rare radiometric observations from aircraft can provide ice surface temperature and a routine for rapid assimilation of these data should be developed. This prompts the need for a numerical model at least for diagnosing ice/snow surface temperature as a function of meteorological inputs.

It must be pointed out that a drag coefficient concept is still needed to enable us to obtain the surface stress from the surface wind; efforts must therefore continue to parameterize it. For instance, an alternative method would be to scale the surface wind computation of the Perfect Prog procedure of Joffre (1983b) or any other with the ECMWF 10-m wind in order to obtain the 1-m wind and thus the stress without knowledge of stability (see Fig. 4).

Yet, no studies have been performed to test the sensitivity of the different oceanographic models to establish which, of V_s , V_1 , V_g , $\langle V \rangle$, $V(h)$ or W_{LW} wind concepts, is the best approach for the model in question since they may have an internal structure (numerical schemes, time-scales, damping factors, etc.) which favours or repulses one or several of the different wind approaches.

Finally, the development of numerical or statistical methods must not let us forget that the real test lies with case studies. While previous experiments had stressed the vertical structure of processes at one point, the next generation of field experiments should concentrate on the horizontal variability of the flow and the transfer on the mesoscale. Such experiments would require several observation ships, remote sensing techniques and co-operation between several interested Institutes.

ACKNOWLEDGEMENTS: First of all I want to thank Dr. P. Mälkki, who initiated the whole project and who has given me his unstinted support throughout the project. The enthusiastic participation of the staff of the IMR in the two large field experiments enabled me to gather a very valuable volume of data, without which this research would have been impossible. Professors S.A. Kitaigorodskii and E. Holopainen were a continuous source of support with their interest in and their comments on the scientific aspects of the work. I also appreciate the cooperation of the SMHI and FMI, and especially of B. Tammelin, for assisting me in the field experiments with personnel and material. I have enjoyed many discussions with Dr. M. Leppäranta, my colleague on the project. My special thanks are due to all those who assisted me in the tedious data analysis: S. Pietikäinen, A. Kalla, R. Hietala, J. Vainio and especially T. Laurila, who also provided his processed Kemi data. I thank Mrs. G. Häkli for her patient and skilful revision of the English of all my manuscripts. M. Leppäranta, K. Eerola, P. Kukkonen, M. Alestalo, P. Mälkki and Professor Holopainen gave constructive comments on this manuscript.

Finally, but not least, I should like to record my debt to the Board of Navigation for their confidence in the project and their financial support.

REFERENCES

Aagaard, K., 1969: "Relationship between geostrophic and surface winds at Weather Ship M". J. Geophys. Res., 74, 3440-3442.

Andreas, E.L., Paulson, C.A., Williams, R.M., Lindsay, R.W., and J.A. Businger, 1979: "The turbulent heat flux from Arctic leads". Boundary-Layer Meteor., 17, 57-91.

Arya, S.P.S., 1973: "Contribution of form drag on pressure ridges to the air stress on Arctic ice". J. Geophys. Res., 78, 7092-7099.

Arya, S.P.S., 1975: Comments on "The influence of geostrophic shear on the cross-isobar angle of the surface wind". Boundary-Layer Meteor., 8, 239-242.

Arya, S.P.S., 1977: "Suggested revisions to certain boundary layer parameterization schemes used in atmospheric circulation models". Monthly Wea. Rev., 105, 215-227.

Arya, S.P.S., 1978: "Comparative effects of stability, baroclinity and the scale-height ratio on drag laws for the atmospheric boundary layer". J. Atmos. Sci., 35, 40-46.

Arya, S.P.S., and J.C. Wyngaard, 1975: "Effect of baroclinicity on wind profiles and the geostrophic drag law for the convective planetary boundary layer". J. Atmos. Sci., 32, 767-778.

Blanc, T.V., 1983: "A practical approach to flux measurements of long duration in the marine atmospheric surface layer". J. Clim. Appl. Meteor., 22, 1093-1110.

Bonner, W.D., and J. Paegle, 1970: "Diurnal variations in boundary layer winds over the south-central United States in summer". Monthly Wea. Rev., 98, 735-744.

Brown, R.A., and W.T. Liu, 1982: "An operational large-scale marine planetary boundary layer model". J. Appl. Meteor., 21, 261-269.

Burt, W.V., Cummings, T., and C.A. Paulson, 1974: "The mesoscale wind field over the ocean". J. Geophys. Res., 79, 5625-5632.

Busch, N.E., Chang, S.W., and R.A. Anthes, 1976: "A multi-level model of the planetary boundary layer suitable for use with mesoscale dynamic model". J. Appl. Meteor., 15, 909-919.

Chamberlain, A.C., 1983: "Roughness lengths of sea, sand and snow". Boundary-Layer Meteor., 25, 405-409.

Feldman, U., Howarth, P.J., and J.A. Davies, 1979: "Estimating the surface wind speed over drifting pack ice from surface weather charts". Boundary-Layer Meteor., 16, 421-429.

Feldman, U., Howarth, P.J., and J.A. Davies, 1981: "Estimating surface wind direction over drifting open pack ice". J. Geophys. Res., 86, 8117-8120.

Garnich, N.G., and S.A. Kitaigorodskii, 1978: "On the theory of the deepening of the upper quasi-homogeneous ocean layer owing to the processes of purely wind-induced mixing". Izv. Atmos. Ocean. Phys., 14, 748-755.

Hasse, L., 1974: "On the surface to geostrophic wind relationship at sea and the stability dependence of the resistance law". Contr. Atmos. Phys., 47, 45-55.

Hasse, L., 1976: "A resistance-law hypothesis for the non-stationary advective planetary boundary layer". Boundary-Layer Meteor., 10, 393-407.

Hasse, L., and V. Wagner, 1971: "On the relationship between geostrophic and surface wind at sea". Monthly Wea. Rev., 99, 255-260.

Holton, J.R., 1967: "The diurnal boundary-layer wind oscillation above sloping terrain". Tellus, 19, 199-205.

Hoxit, L.R., 1974: "Planetary boundary layer winds in baroclinic conditions". J. Atmos. Sci., 31, 1003-1020.

Häkkinen, S., 1980: "Computation of sea level variations during December 1975 and 1 to 17 September 1977 using numerical models of the Baltic Sea". Dt. Hydrogr. Z., 33, 158-175.

Joffre, S.M., 1978: "Studies of the winter-time boundary layer over the Baltic Sea based on pilot balloon soundings". Merentutkimuslaitoksen Julk., 243, 3-62.

Joffre, S.M., 1981: "The physics of the mechanically-driven atmospheric boundary layer as an example of [illegible] ice interactions". Report No. 20, Univ. Helsinki, [illegible] "Meteorology, 75 pp.

Joffre, S.M., 1982a: "Assessment of the separate effects of baroclinicity and thermal stability in the atmospheric boundary layer over the sea". Tellus, 34, 567-578.

Joffre, S.M., 1982b: "Momentum and heat transfers in the surface layer over a frozen sea". Boundary-layer Meteor., 24, 211-229.

Joffre, S.M., 1982c: "The atmosphere-ice-water interface". In The Arctic Ocean, Ed. L. Rey, Macmillan Publ., London, 97-111.

Joffre, S.M., 1983a: "Determining the form drag contribution to the total stress of the atmospheric flow over ridged sea ice". J. Geophys. Res., 88, 4524-4530.

Joffre, S.M., 1983b: "Surface wind predictions and boundary layer mass flow". Geophysica, 20, 51-70.

Joffre, S.M., 1984a: "Power laws and the empirical representation of velocity and directional shear". J. Clim. Appl. Meteor., 23, (in press).

Joffre, S.M., 1984b: "Effects of local acceleration and baroclinity on the mean structure of the atmospheric boundary layer over the sea". Boundary-Layer Meteor., (in press).

Joffre, S.M., and L. Makkonen, 1981: Comments on "Comparison of mean wind speeds and turbulence at a coastal site and an offshore location". J. Appl. Meteor., 20, 835-838.

Kahma, K., and M. Leppäranta, 1981: "On errors in wind speed observations on R/V Aranda". Geophysica, 17, 155-165.

Kantha, L.H., Phillips, O.M., and R.S. Azad, 1977: "On turbulent entrainment at a stable density interface". J. Fluid Mech., 79, 753-768.

Kato, H., and O.M. Phillips, 1969: "On the penetration of a turbulent layer into stratified fluid". J. Fluid Mech., 37, 643-655.

Kau, W.S., Lee, H.N., and S.K. Kao, 1982: "A statistical model for wind prediction at a mountain and valley station near Anderson Creek, California". J. Appl. Meteor., 21, 18-21.

Kitaigorodskii, S.A., 1979: "Review of the theories of wind-mixed layer deepening". In Marine Forecasting, Ed. J. Nihoul, Elsevier, 1-33.

Kukkonen, P., 1982: "The use of ECMWF DMO wind and cloudiness forecasts in Finland", Finnish Meteorological Institute, Internal Report, 12 pp.

Kullenberg, G., 1977: "Entrainment velocity in natural stratified vertical shear flow", Estuarine and Coastal Mar. Sci., 5, 329-338.

Lange, A., 1973: "Statistical surface wind prediction in Finland". Finnish Meteorological Institute, Tech. Report No. 6, 23 pp.

Leppäranta, M., 1981: "An ice drift model for the Baltic Sea". Tellus, 33, 583-596.

Macklin, S.A., 1983: "Wind drag coefficient over first-year sea ice in the Bering Sea". J. Geophys. Res., 88, 2845-2852.

Mahrt, L., 1974: "Time dependent, integrated planetary boundary layer flow". J. Atmos. Sci., 31, 457-464.

Mahrt, L., 1975: "The influence of momentum advections on a well-mixed layer". Quart. J. R. Met. Soc., 101, 1-11.

Mahrt, L., André, J.C., and R.C. Heald, 1982: "On the depth of the nocturnal boundary layer". J. Appl. Meteor., 21, 90-92.

Niiler, P.P., and E.B. Kraus, 1977: "one-dimensional models of the upper ocean". In Modelling and Prediction of the Upper Layers of the Ocean, Ed. E.B. Kraus, Pergamon Press, Oxford, 143- 172.

Orlanski, I., 1975: "A rotational subdivision of scales for atmospheric processes". Bull. Amer. Meteor. Soc., 56, 527-530.

Pease, C.H., Salo, S.A., and J.E. Overland, 1983: "Drag measurements for first-year sea ice over a shallow sea". J. Geophys. Res., 88, 2853-2862.

Phillips, O.M., 1977: "Entrainment". In Modelling and Prediction of the Upper Layers of the Ocean, Ed. E.B. Kraus, Pergamon Press, Oxford, 92-101.

Pinty, B., and H. Isaka, 1982: "Analysis of the diurnal oscillation of surface geostrophic wind over Western Europe". Tellus, 34, 545-554.

Pollard, R.T., Rhines, P.B., and R.O.R.Y. Thompson, 1973: "The deepening of the wind-mixed layer". Geophys. Fluid Dyn., 3, 381-404.

Rinne, J., Launiainen, J., Alestalo, M., Grönvall, H., Kukkonen, P., Joffre, S.M., and J. Jokinen, 1984: "Aallokko-ryhmän loppuraportti". Helsinki, 7 pp.

Roth, R., 1981: "The daily variation of the geostrophic wind speed". Contr. Atmos. Phys., 54, 101-106.

Stull, R.B., 1983a: "A heat-flux history length scale for the nocturnal boundary layer". Tellus, 35A, 219-230.

Stull, R.B., 1983b: "Integral scales for the nocturnal boundary layer. Part 1: Empirical depth relationships". J. Clim. Appl. Meteor., 22, 673-686.

Tennekes, H., and A.G.M. Driedonks, 1981: "Basic entrainment equations for the atmospheric boundary layer". Boundary-Layer Meteor., 20, 515-531.

Topham, D.R., Perkin, R.G., Smith, S.D., Anderson, R.J., and G. den Hartog, 1983: "An investigation of a polynya in the Canadian Archipelago, 1: Introduction and oceanography". J. Geophys. Res., 88, 2888-2899.

Weisberg, R.H., and L.J. Pietrafesa, 1983: "Kinematics and correlation of the surface wind field in the South Atlantic Bight". J. Geophys. Res., 88, 4593-4610.

Wucknitz, J., 1980: "Flow distortion by supporting structures". In Air-Sea Interaction, Instruments and Methods, F. Dobson and L. Hasse, Eds., Plenum Press, 605-626.

Yu, T., 1978: "Determining height of the nocturnal boundary layer". J. Appl. Meteor., 17, 28-33.

ISBN 951-46-8314-5